Mon. Not. R. Astron. Soc. **302,** 457–481 (1999)

Magnetic cycles of HR 1099 and LQ Hydrae

J.-F. Donati★
Laboratoire d'Astrophysique, Observatoire Midi-Pyrénées, F–31400 Toulouse, France

Accepted 1998 August 17. Received 1998 August 17; in original form 1998 March 23

ABSTRACT

We present in this paper a 6-yr time series of magnetic (and brightness) surface images of the K1 subgiant of the RS CVn system HR 1099 (=V711 Tauri) and of the young K0 dwarf LQ Hydrae, reconstructed (with the help of a dedicated maximum entropy image reconstruction software) from Zeeman–Doppler imaging observations collected at the Anglo-Australian Telescope.

All the stellar magnetic images that we reconstruct host at least one high-contrast feature in which the field is predominantly azimuthal, thus confirming that such surface structures (already detected in previous similar studies) are indeed real. We take this as strong evidence that dynamo processes of late-type rapid rotators operate throughout the *whole stellar convective envelope*, rather than being confined to an interface layer between the convective and radiative zones as in the Sun. The latitudinal polarity pattern of azimuthal and radial fields that we observe at the surface of both stars suggests that these magnetic regions respectively reveal the *toroidal and poloidal components of the large-scale dynamo field*. The spatial structure of these two magnetic field components becomes increasingly more complex (with higher axisymmetric spherical harmonic degrees) for larger rotation rates and deeper convective zones. The strength of the toroidal and poloidal components is typically a few hundred G, more than *two orders of magnitude stronger* than in the Sun. Long-term evolution of the toroidal and poloidal components of the large-scale field is clearly detected in our time series.

We also report the detection of small fluctuations in the orbital period of HR 1099, with a peak-to-peak amplitude of about 36 ± 1 s (i.e. 0.015 per cent) and a period of about 18 ± 2 yr (assuming sinusoidal variations around the nominal value). The most plausible way of explaining such fluctuations is that the quadrupole moment of the K1 subgiant is varying with time, and that this modulation is driven by the magnetic activity cycle of the primary star itself (through a periodic exchange between kinetic and magnetic energy within the convective zone). It provides in particular an independent confirmation that a dynamo operates within the whole convective zone, and suggests that the average azimuthal field in the convective envelope is of the order of 6 kG.

Key words: line: profiles – stars: activity – binaries: general – stars: imaging – stars: magnetic fields – stars: rotation.

1 INTRODUCTION

The new technique of Zeeman–Doppler imaging (ZDI, Semel 1989) now offers the opportunity of studying magnetic topologies of rapidly rotating cool active stars. As demonstrated with detailed numerical simulations (Brown et al. 1991; Donati & Brown 1997), ZDI allows one to map magnetic regions on stellar surfaces, but also informs us about the direction of field lines within these regions. It thus represents an important step forward with respect to conventional polarimetric methods (measuring only the line-of-sight projected field vector averaged over the whole visible hemisphere, e.g. Borra & Landstreet 1980) or with the so-called 'Robinson technique' (estimating the fraction of the stellar surface covered with magnetic field and the mean field strength within them, Robinson 1980), which both turn out to contain relatively little information about the actual field topology.

ZDI thus opens a vast new field of research, enabling us for instance to study in a large sample of active stars where on the stellar surface magnetic spots tend to form and migrate preferentially, how magnetic topologies depend on stellar fundamental

★ E-mail: donati@obs-mip.fr

parameters such as rotation rate, and how they vary on a time-scale of several years. This in turn should help us in testing, constraining and generalizing on stars other than the Sun dynamo theories that have been elaborated for the Sun only, for instance by identifying where dynamo processes take place preferentially (e.g. in an overshoot layer between the radiative and convective envelopes as on the Sun or distributed throughout the whole convective zone) or what kind of dynamo is in operation ($\alpha\Omega$, $\alpha^2\Omega$ or α^2).

Thanks to ZDI, circularly polarized Zeeman signatures have been detected at the surface of 20 different objects already, including three pre-main-sequence stars, four main-sequence stars (three of which are still fairly young) and 13 more evolved stars (Donati, Semel & Rees 1992a; Donati et al. 1997). For two of them, namely the young dwarf AB Doradus [Donati & Cameron 1997; Donati et al. 1999 (Paper I, this issue)] as well as the evolved K1 component of the RS CVn system HR 1099=V711 Tauri (Donati et al. 1992b), magnetic maps are already published in the literature. With a rotation period of about half a day, the first one belongs to the class of ultra-fast rotators in the phase of completing their contraction towards the main sequence. Although quite far away from the main sequence already, the K1 subgiant of HR 1099 is still a rather fast rotator (with a rotation period of about 2.8 d) thanks to the orbital to spin angular momentum transfer ensured through tidal coupling. One of the most intriguing feature of these images is that they all include magnetic regions of *mainly azimuthal* field, the *polarity* of which is roughly independent of longitude. From these initial results, the authors speculated that these regions actually reveal the presence of a large-scale axisymmetric azimuthal field structure distributed throughout the whole convective zone (Donati & Cameron 1997; Donati et al. 1999).

In order to test this idea further, more magnetic maps are obviously needed, both for one given star observed during a long time sequence, and for a small sample of active objects selected at different evolutionary stages. This paper first presents five new magnetic maps of the evolved K1 component of HR 1099 obtained at epochs 1991.96, 1992.94, 1993.99, 1995.94 and 1996.99. When coupled with the image published already (corresponding to epoch 1990.9), we obtain a 6-yr time base on which long term evolution of the magnetic topology of HR 1099 can be analysed. We also present herein five magnetic images (obtained at the same five epochs as HR 1099) for a third object, the cool dwarf LQ Hydrae. With a rotation period of 1.6 d, this star is still fairly young (given its high lithium content) and presumably arrived only very recently on the main sequence. Note that the fragmentary results from a very preliminary analysis published in conference proceedings (Donati 1996a, 1996b) are superseded by the new and final ones presented herein.

After a brief description of the spectropolarimetric data gathered for this study and the imaging tools used to convert them into surface magnetic maps of HR 1099 and LQ Hya (Section 2), we will describe the different images we obtained (Sections 3 and 4) and discuss the implications for dynamo theories (Section 5).

2 OBSERVATIONS AND MODELLING TOOLS

2.1 Data collection and reduction

Observations were recorded at the Anglo-Australian Telescope, with a visitor polarimeter mounted at Cassegrain focus and feeding the UCL Echelle Spectrograph (UCLES) through a double fibre (Semel & Li 1995; Donati et al. 1997). All observations we use in this paper are already reported in Donati et al. (1997), except for those obtained in 1996 December the log for which is given in Table 1. The slightly different setup used for this last run is described in Donati et al. (1999). Spectral resolution ranges between 55 000 and 75 000 depending on the epoch.

All frames were processed with ESPRIT, a dedicated package for optimal extraction of échelle spectropolarimetric observations (Donati et al. 1997). Altogether, 251 individual subexposures on HR 1099 were collected with different azimuths of the quarter-wave plate, producing 64 Stokes V (processed from groups of two or four individual subexposures, see Donati et al. 1997 for details) and 251 Stokes I spectra of this target. Note that one Stokes I spectrum (corresponding to the first subexposure collected on 1996 December 25 at evening twilight) was rejected owing to strong contamination by scattered sunlight. On LQ Hya, 116 and 31 Stokes I and V spectra were obtained throughout the different runs.

For this analysis, we used least-squares deconvolution (LSD), a new cross-correlation technique developed by Donati et al. (1997), which extracts information from every moderate to strong spectral features in the recorded wavelength domain. The LSD unpolarized (Stokes I) and circularly polarized (Stokes V) profile we obtain with this method can be roughly described as a weighted average of all profiles involved in the analysis. In particular, its relative noise level is considerably reduced compared to that of each single line of the original spectrum. Moreover, as demonstrated in Donati &

Table 1. Journal of 1996 December observations. For both stars, we list here the observing date (second column), the number of exposure sequences collected on this object at this date ($n_{\rm exp}$, third column), together with the range of corresponding Julian dates (fourth column), total exposure times ($t_{\rm exp}$, fifth column) and *peak* signal-to-noise (S/N) ratios per 3 km s^{-1} pixel (sixth column). The two last columns indicate respectively the range of S/N ratios in the associated least-squares deconvolved spectra and the corresponding multiplex gains in S/N ratio.

Object	Date	$n_{\rm exp}$	JD (2,450,000+)	$t_{\rm exp}$ (sec.)	S/N (pixel^{-1})	S/N$_{\rm LSD}$ (pixel^{-1})	Multiplex gain
HR 1099	1996 Dec. 24	3	441.9123/442.0951	600/1200	500/750	14100/22100	28/29
HR 1099	1996 Dec. 25	1	442.9023	800	550	14600	27
HR 1099	1996 Dec. 26	2	443.9736/444.0882	1200	410/470	12300/14700	30/31
HR 1099	1996 Dec. 27	2	444.9187/445.1064	800	330/440	8500/12100	26/28
HR 1099	1996 Dec. 29	2	446.9120/447.1115	800	440/530	12100/15500	28/29
LQ Hya	1996 Dec. 24	3	442.0615/442.2457	1200	130/220	3500/6600	26/30
LQ Hya	1996 Dec. 25	1	443.0741	800	180	4600	26
LQ Hya	1996 Dec. 26	4	444.0688/444.1911	1200	93/180	1200/4400	13/24
LQ Hya	1996 Dec. 27	2	445.0550/445.2305	800	110/210	1800/5300	16/25
LQ Hya	1996 Dec. 28	1	446.2006	1200	290	8000	28
LQ Hya	1996 Dec. 29	2	447.0593/447.2144	800	180/210	4300/5400	24/26

Cameron (1997), LSD conserves the shape of a pure rotational profile to a very good accuracy, implying that any deviation observed in LSD profiles from this reference level can be considered as real and, in our particular case, ready to be interpreted in terms of surface brightness/magnetic inhomogeneities. The list of spectral lines available for LSD (and in particular their wavelengths, relative central depths and Landé factors) are obtained from a full LTE spectral synthesis using Kurucz's (1993) model atmospheres (a K1IV and a K0V atmosphere for HR 1099 and LQ Hya respectively), and selecting only those features whose relative central depth (prior to rotation or macroturbulence broadening) exceeds 40 per cent. In our particular case, the total number of lines used in the analysis ranged from 440 up to 2100, depending on the epoch and spectral type (Donati et al. 1997). All LSD profiles shown in Sections 3 and 4 are normalized to mean weights of 0.7 and 500 nm for Stokes *I* and Stokes *V* data respectively.

2.2 Brightness and magnetic surface imaging

To convert sets of rotationally modulated Stokes *V* and *I* profiles into magnetic and brightness stellar surface maps, we use the dedicated image reconstruction code of Brown et al. (1991) and Donati & Brown (1997), which implements Skilling & Bryan's (1984) algorithm for maximum entropy optimization problems.

The magnetic model we chose is that of Donati & Brown (1997), which assumes that the intrinsic profile is Gaussian and constant over the stellar surface, and that the weak field approximation holds. Although very simple, this model is found to be perfectly adequate for describing LSD Stokes *V* profiles averaged over several thousand individual spectral features as demonstrated in Donati & Cameron (1997) and Donati et al. (1997). In particular, observations of very slowly rotating and weakly magnetized Ap stars indicate that the weak-field regime holds, for LSD profiles, up to field strengths of several kG (Donati & Cameron 1997). The quantities we reconstruct are the three components of the magnetic field vector in spherical coordinates (i.e. radial, meridional and azimuthal field), weighted by potential surface inhomogeneities in brightness, local magnetic field occupancy and central depth of true intrinsic profile.

Numerical simulations by Donati & Brown (1997) demonstrate that complex magnetic distributions (featuring in particular spots with various field orientations) can adequately be recovered from sets of rotationally modulated Stokes *V* signatures. While the *trajectory* of Stokes *V* signatures across the line profile (as derived from dynamic spectra) gives access to the *location* of the corresponding magnetic regions on the stellar surface (just as in conventional Doppler imaging), the *amplitude modulation* of these Zeeman signatures in their transit through the line profile yields (to a certain extent) the *orientation of field lines* within the magnetic regions. Donati & Brown (1997) demonstrate in particular that magnetic regions in which the field is *azimuthal* can be well distinguished from those in which the field is either radial or meridional; however, they find that ZDI (from circular spectropolarimetry alone) can suffer potentially important crosstalk from radial to meridional field components (and vice versa) in the particular case of low-latitude features (i.e. with a latitude lower than the stellar inclination angle *i*), especially at low stellar inclination angles ($i < 45^\circ$).

Donati & Brown (1997) also study the impact of poor rotational phase sampling on the reconstructed magnetic image, a problem one has to deal with when observing stars like the K1 subgiant of HR 1099, the rotation period of which is close to a small integer number of days (see Section 3). In that respect, they demonstrate that phase sampling on time-scales of a few per cent of the rotation cycle also contains very rich information for imaging, and sometimes partially compensates for the poor overall coverage of the rotation cycle. Also worth noting is the fact that, for a given magnetic region at the surface of the star, the associated Stokes *V* signature reaches a maximum amplitude when the region crosses the meridian, if field lines within this region are radially or meridionally oriented. For a magnetic region with azimuthally oriented field lines on the opposite, the Stokes *V* signature is strongest about 0.2 rotation cycle away from the phase of meridian crossing and very weak close to the phase of meridian crossing (Donati & Brown 1997). It implies in particular that, in case of poor phase coverage, ZDI should be mostly sensitive to radial/meridional field features located closest to the phases of observations, and to the azimuthal field ones located about 0.2 rotation cycle away from the phases of observations. All such properties should be kept in mind when interpreting the reconstructed magnetic maps presented in Sections 3 and 4.

Although the present paper focuses essentially on magnetic imaging of HR 1099 and LQ Hya from Stokes *V* data sets, only modest additional effort was required to derive simultaneous brightness images of both stars from Stokes *I* data sets. The imaging model we used is the two-component model of Cameron (1992) which aims at reconstructing for each point of the stellar surface a quantity f describing the local fraction of the stellar surface occupied by cool spots. This quantity, varying from 0 (no spot) to 1 (maximum spottedness), is referred to as 'spot occupancy' in the following. LSD profiles of very slowly rotating standard stars (δ Eri, Gl 176.3 and Gl 367) were used as template profiles describing the spectral contribution of the photosphere and spot respectively, just as in Donati & Cameron (1997) and Donati et al. (1999). In this context, an integrated model profile associated with a given stellar image viewed at a given rotational phase can be obtained by shifting in velocity and adding up together the spectral contributions of all image pixels. Note that no photometric data were used to constrain further this type of reconstruction, implying that the brightness images we recover should only be considered as first-order estimates. They should be at least accurate enough for our particular purpose, which consists in nothing more than comparing the approximate location of brightness and magnetic inhomogeneities (see the following sections).

Note that brightness maps were not used to correct magnetic images for brightness inhomogeneities. As emphasized already in Donati & Cameron (1997), a reconstructed brightness map is not the true brightness map (given all blurring processes it is subject to for instance) so that it is hard to know whether taking it into account for the magnetic inversion degrades or improves the reconstructed field image. Keeping both Stokes *I* and *V* reconstructions fully independent has the additional advantage of avoiding any possible crosstalk between the resulting maps.

We introduce several global parameters to characterize the reconstructed distributions. One can first define the *total spottedness* (respectively *mean field strength*) of a brightness (respectively magnetic field) distribution by summing up over all image pixels $p_i f_i$ (respectively $p_i B_i$) where p_i and f_i (respectively B_i) denote the fractional area and local spot occupancy (respectively modulus of local field vector) at image pixel *i*. One can also define brightness (respectively magnetic) *filling factors* by computing thresholded versions of the reconstructed distributions (in which all f_i or B_i pixel values below a given threshold are set to zero), thresholds being set such as the spottedness (respectively mean field strength) of the thresholded images are half that of the original images. The *filling*

factors of the original distributions are then obtained by summing up the fractional area of all cells in the thresholded image for which f_i (respectively B_i) pixel values are non-zero. These filling factors thus represent the fractional stellar surface covered by the darkest (respectively most magnetic) regions that enclose 50 per cent of the total spottedness (respectively mean field strength) altogether.

3 THE RS CVN SYSTEM HR 1099

3.1 Preparing the data set

3.1.1 Removing the contribution of the secondary star

In order to construct sets of rotationally modulated Stokes *I* and *V* profiles for the primary component of HR 1099, one first needs to derive accurate orbital parameters for the secondary star. This is necessary for precisely removing, at conjunction phases, the spectral contribution of the companion from the profiles of the primary star.

This correction is essential for Stokes *I* data. To achieve it, we measure the radial velocity of the secondary star in each LSD Stokes *I* profiles and for each epoch (using in particular the method of Donati et al. 1992b at conjunction phases) and solve for all orbital elements simultaneously. As the eccentricity we find is always smaller than 0.01 (i.e. within the measurement error bars, typically equal to 0.004 for each epoch), we assume a circular orbit, in agreement with previous findings of Fekel (1983) and Donati et al. (1992b). The results (summarized in Table 2) indicate that, while the system radial velocity γ and semi-amplitude of secondary star velocity curve K_s remain constant (and respectively equal to 14.9 and 63.1 km s^{-1} on average, in perfect agreement with the original estimates of Fekel 1983) within the error bars, the orbital phase of the first conjunction ϕ_0 is slowly but very significantly varying with time (see Fig. 1). Note that the very high accuracy to which ϕ_0 is measured essentially reflects the high precision radial velocities one can obtain near conjunction phases from sequences of consecutive exposures using the method of Donati et al. (1992b).

These fluctuations will be discussed in more details further in the paper (see Section 5.3). Meanwhile, we use the results of Table 2 to compute the radial velocity of the secondary star for each observed phase and at each epoch, and remove the spectral contribution of the secondary star (assumed Gaussian) from all individual LSD Stokes *I* profiles of the system.

This correction is much less important for Stokes *V* profiles, as Zeeman signatures from the secondary star are always very small (Donati et al. 1997). We nevertheless checked whether the G5 companion exhibits a non-zero phase-averaged Zeeman signature that we could subtract from the Stokes *V* profiles of the primary star at conjunction phases. We actually observe that the Stokes *V* profiles of the G5 star away from conjunction phases are roughly constant in shape with rotational phase and epoch throughout the whole observing period (see Fig. 2), with a peak-to-peak relative amplitude of about 0.07 per cent with respect to the secondary star continuum (or 0.03 and 0.02 per cent with respect to the primary and system continua respectively). This mean Zeeman signature (whose putative origin is discussed in Section 5.1) corresponds to an average longitudinal field of about 10 G. All LSD Stokes *V* profiles of the primary star at conjunction phases were corrected from this circularly polarized contribution from the secondary star. Note that this correction is sufficiently small (5 to 10 times smaller than the Stokes *V* signatures of the K1 subgiant) and affects a small enough number of phases that its impact on the imaging process is extremely small (magnetic topologies reconstructed from the

Table 2. Orbital parameters (velocity amplitude K_s, systemic velocity γ and orbital phase of first conjunction ϕ_0 in the ephemeris of Fekel 1983) for the secondary star of HR 1099, assuming a circular orbit. The rms error bars on K_s are γ are equal to 0.2 and 0.5 km s^{-1} respectively, while that on ϕ_0 is 0.0004. Note that the 1990.9 entry corresponds to a new fit to the radial velocities of the secondary star listed in Donati et al. (1992b).

Epoch	K_s km s^{-1}	γ km s^{-1}	ϕ_0
1990.9	62.8	−15.4	+0.0077
1991.96	63.3	−14.9	+0.0030
1992.94	63.2	−15.0	−0.0023
1993.99	63.1	−15.0	−0.0117
1995.94	63.0	−14.9	−0.0300
1996.99	63.1	−14.3	−0.0378

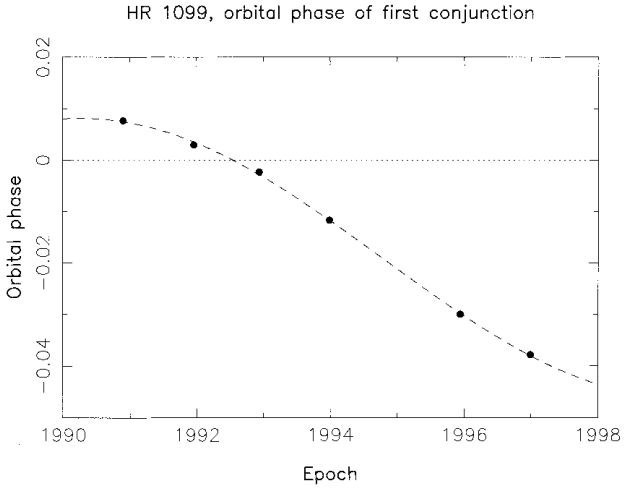

Figure 1. Time variation of the orbital phase of first conjunction, for the RS CVn system HR 1099 (dots), with an 18-yr period sinusoidal fit to the data (dashed curve). The symbol size approximately corresponds to a 3σ error bar.

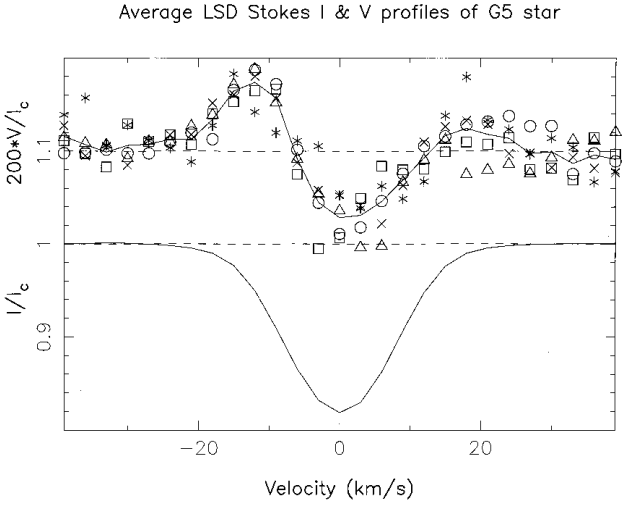

Figure 2. LSD Stokes *I* (bottom curve) and *V* (top curve) profiles of the G5 secondary star, averaged over all phases and epochs. The phase-averaged Stokes *V* signatures at each epoch are depicted with different symbols (asterisks for 1991 December, open circles for 1992 December, crosses for 1993 December, squares for 1995 December and triangles for 1996 December).

corrected data set are virtually identical to those derived from the uncorrected one).

As we did not have access to simultaneous photometry for all epochs, we expanded all LSD Stokes *I* and *V* profiles (as corrected for the pollution of the secondary component) by an average factor of 1.4, corresponding to the average brightness ratio between the binary system and primary star (Henry et al. 1995).

All rotational phases listed in the following sections are computed with Fekel's original ephemeris (1983) to allow easier comparison of surface images with other contemporaneous studies (e.g. Vogt et al. 1998). The small time intervals over which each data set was collected (always shorter than 2.1 rotation cycles) ensures in particular that potential internal phase inconsistency caused by yearly variations in photometric period (i.e. to surface differential rotation, e.g. Henry et al. 1995) is always smaller than 1 per cent of the rotational cycle.

3.1.2 *Estimating imaging parameters*

The next step for building rotationally modulated Stokes *I* and *V* data sets is to recenter all primary star profiles on to zero radial velocity, i.e. to obtain an accurate estimate of the semi-amplitude of the primary star velocity curve K_p. To achieve this, we do not construct the velocity curve of the primary star (as we did for the secondary); radial velocities are very difficult to estimate accurately for this system component owing to the presence of large cool surface structures that strongly distort the shape of the Stokes *I* line profiles. We prefer to use a different technique, consisting in running several reconstructions for data sets obtained with different values of K_p, and take the one that minimizes the information content of the reconstructed image as the most likely (as prescribed by Cameron & Unruh 1994 for a similar situation). We obtain for K_p a value of 50.0 ± 0.5 km s^{-1}, in good agreement with the original estimate of Fekel (1983).

All other imaging parameters, and in particular the inclination angle i and the projected rotational velocity $v \sin i$, can be derived with the same method. Averaging results from all different epochs, we obtain most likely estimates of $i = 40 \pm 5°$ and $v \sin i = 41 \pm 0.5$ km s^{-1}. Note that this second parameter is in perfect agreement with that found by Donati et al. (1992b) and with the new estimate of Vogt et al. (1998). The inclination angle is slightly larger than the commonly used value of $33 \pm 2°$ proposed by Fekel (1983).

From the very new and accurate distance estimate obtained for HR 1099 (29.0 ± 0.7 pc) by the *Hipparcos* astrometry satellite (Perryman et al. 1997), it is possible to obtain a third independent value of the inclination angle. Given the maximum brightness level observed for this object in the last 20 yr ($m_V = 5.7$ for the system at epoch 1984.8, i.e. 6.00 ± 0.07 for the primary star assuming a secondary component with $m_V = 7.2 \pm 0.2$, Henry et al. 1995) and the area of the polar spot it continually hosts (about 10 per cent of the total stellar surface, i.e. 15–20 per cent of the visible hemisphere, Vogt et al. 1998), we conclude that the unspotted *V* magnitude of the K1 subgiant is 5.80 ± 0.10. From the effective temperature (4750 ± 100 K) and the associated bolometric correction (-0.50 ± 0.05, Kurucz 1993), we then obtain a bolometric magnitude of 3.0 ± 0.2 and therefore a radius of $3.3^{+0.5}_{-0.4}$ $R_\odot$. The measured $v \sin i$ (see previous paragraph) and the rotation period of 2.83774 d imply a line-of-sight projected radius 2.30 ± 0.05 $R_\odot$ and therefore indicate that the inclination angle should be equal to 44°, with possible values ranging from 36° up to 54°.

Inclination angles larger than 40° (yielding masses smaller than 0.7 $M_\odot$ for the secondary component whose temperature is estimated to be 5500 K, Fekel 1983) are somewhat difficult to reconcile with modern stellar structure models (e.g. Bressan et al. 1993; Charbonnel et al. 1996) though, which predict that such stars should never reach effective temperatures larger than 5000 K shortly after leaving the main sequence. The same models also indicate that the logarithmic gravity of the K1 subgiant we derive from the system orbital elements (ranging from 3.3 to 3.2 for inclination angles of 35° to 50°) can only be reconciled with the observed effective temperature for masses larger than 0.9 $M_\odot$, i.e. for inclination angles lower than 40°.

The value we used for the computations presented in the following sections, 38° (in good agreement with the one obtained from our inversion attempts, see previous paragraphs), is a compromise between the constraints we get from both *Hipparcos* measurements and stellar evolution models. It corresponds to primary and secondary masses of 1.0 and 0.8 $M_\odot$ and radii of 3.7 and 1.1 $R_\odot$ respectively, and to a system separation of about 10.3 $R_\odot$. Although an accurate determination of i is a very important key for deriving precise fundamental parameter estimates for both system components and thus for our general understanding of the system long-term evolution, it is not a crucial issue for the present paper as potential errors of $\pm 10°$ produce only very small differences in the reconstructed images. We therefore stick with this value of i and leave this problem (which requires a detailed spectroscopic analysis of both system components) for a forthcoming study.

All HR 1099 data presented in the following are fitted to a relative noise level of 0.2 per cent (S/N = 500) for LSD Stokes *I* profiles, and to a reduced χ^2 level of 1.6 for LSD Stokes *V* profiles. The total spottedness, mean field strength, brightness and magnetic filling factors the code reconstructs (see last paragraph of Section 2.2 for a definition of these quantities) are respectively equal to 10 per cent, 175 G (except on 1991 December where the mean field strength is only 100 G), 7 per cent and 15 per cent on average.

3.2 1991 December

Fig. 3 presents the resulting spot occupancy maps (called brightness maps in the following) and magnetic images of the K1 subgiant of HR 1099 at epoch 1991.96, along with the associated observed and reconstructed Stokes *I* and *V* data sets. The resulting magnetic images are relatively featureless, with only two regions (a radial field spot at phase 0.62 and an azimuthal field one at phase 0.82) in which the reconstructed field strength exceeds 650 G. Although this may partly be because of both moderate data quality and the small number of available Stokes *V* observations, it probably also reflects the constantly small amplitude of the detected Zeeman signatures at that time (usually smaller than 0.2 per cent peak-to-peak and as low as 0.1 per cent around phase 0.0). The first point worth mentioning already in these magnetic images is the fact that we detect features in which the field is essentially *horizontal*, very similar to what was reported for the same object at epoch 1990.9 by Donati et al. (1992b).[1] As recalled in Section 2.2, azimuthal field features (as opposed to low latitude radial/meridional field ones) are not subject to crosstalk problems in the reconstruction (Donati & Brown 1997) and must therefore be considered as real, even if very intriguing and difficult to explain in the context of the standard solar dynamo theory (see Section 5 for a discussion on this subject).

As expected from the rather short evolution timescales of surface

[1] Note that azimuthal and meridional fields were erroneously called 'toroidal' and 'poloidal' in this paper.

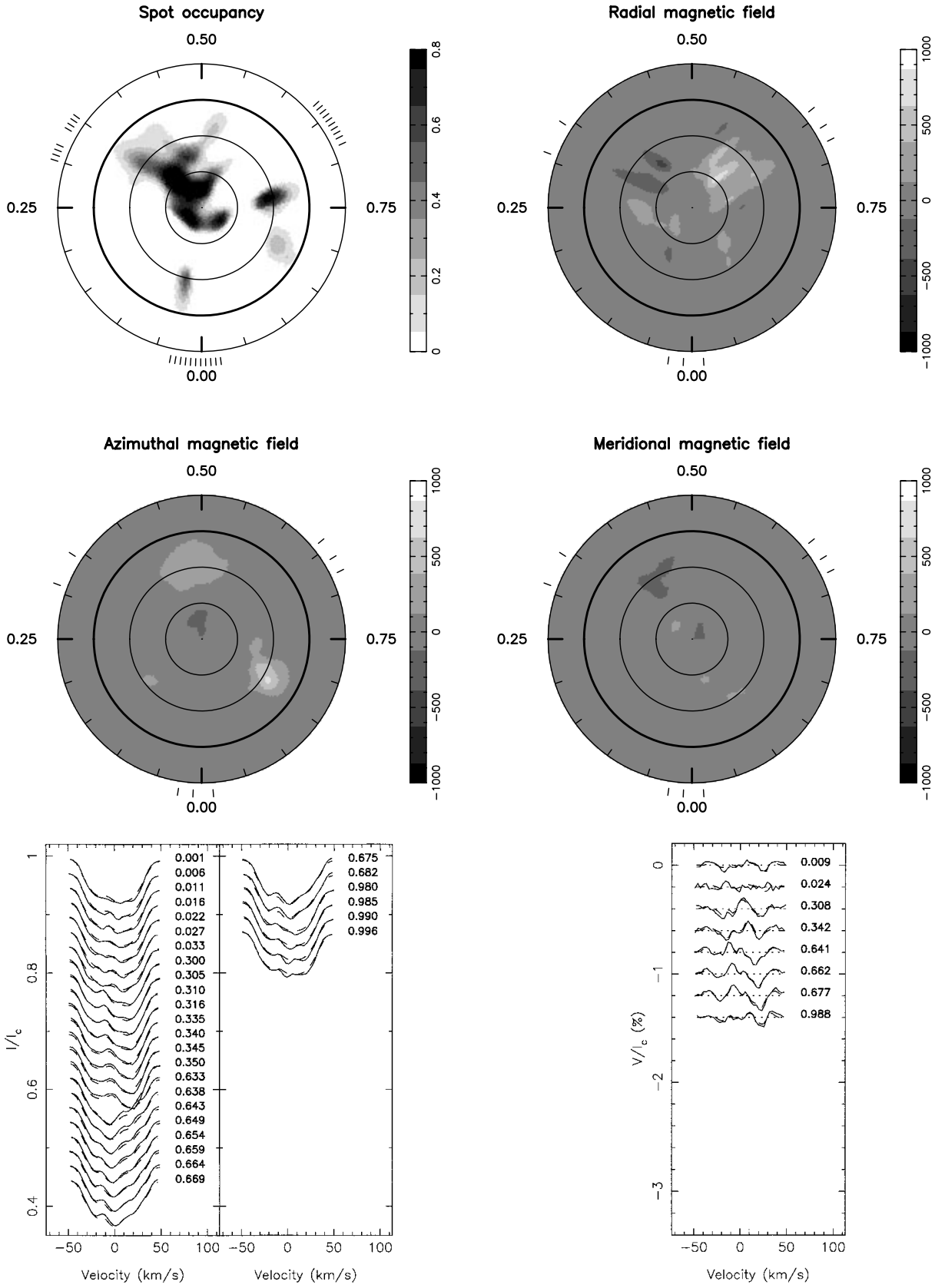

Figure 3. Top panel: Maximum entropy brightness (upper left) and magnetic field images of the K1 subgiant of HR 1099 at epoch 1991.96. These images are flattened polar projections extending down to a latitude of −30° (the bold and thin circles depicting the equator and the 30° and 60° latitude parallels respectively). The radial ticks around (and outside) each plot illustrate the phases at which the star was observed. Positive field values correspond to magnetic vectors directed outward, anticlockwise and poleward for radial, azimuthal and meridional field components respectively (all labelled in G). Bottom panel: maximum entropy fit (dashed line) to the observed (solid line) Stokes *I* (left) and *V* (right) data sets. Rotational phases are indicated right to each profile.

distributions in this object (Vogt et al. 1998), there is no spatial correspondence between the magnetic features detected at epoch 1990.9 by Donati et al. (1992b) and those we reconstruct here for epoch 1991.96. However, it is interesting to note that the *polarity* of the two *azimuthal* field features we detect at low latitude is positive (i.e. counterclockwise field) while that of the very weak one reconstructed close to the pole (if real) is negative, which corresponds precisely to what was observed one year before. The main difference with respect to the 1990.9 image of Donati et al. (1992b) is that weak radial field spots (of mainly positive polarity) are now detected at intermediate latitudes. The only reconstructed meridional field feature (a weak low latitude spot at phase 0.40) has an obvious counterpart at exactly the same location in the radial field map; it is therefore impossible to know whether this feature corresponds to truly meridional field or results from the radial to meridional field crosstalk that low-latitude regions are subject to in low-inclination stars (Donati & Brown 1997). Note that, as predicted in Section 2.2, ZDI detects preferentially the radial/meridional (respectively azimuthal) field features located close to (respectively between) phases of observations when only moderate phase coverage is available.

The major feature we reconstruct in the brightness image is a large high-contrast spot at high latitude (centred on phase 0.38), with at least one low-latitude appendage at phase 0.35. It is in particular quite similar in this respect to the polar spot Vogt et al. (1998) observe for HR 1099 at epoch 1991.90 and 1992.04 (bracketing our observations in time). Note that such a polar feature has constantly been observed on HR 1099 (with a time variable shape though) for more than 15 yr now (Vogt et al. 1998). The smaller spot we reconstruct at phase 0.72 and latitude 30° is also visible in Vogt et al. (1998) results, almost at the same location in the 1992.04 map and in the form of a small polar spot appendage at epoch 1991.90. The low-latitude feature Vogt et al. (1998) reconstruct at phase 0.13 in both maps has no obvious counterpart in our image, likely owing to the lack of observations at that particular phase in our data set.

The main point worth mentioning for the present study is that there seem to be no obvious spatial correlation between brightness and magnetic field inhomogeneities. While some field regions (the two negative radial field spots at phase 0.35 and the positive azimuthal field one at phase 0.82 for instance) are indeed associated with dark spots, some others (like the positive radial field regions at phase 0.62) have no obvious counterpart in the brightness image. One should of course keep in mind that some of the original magnetic flux (that from the darkest regions of the stellar surface in particular) is probably missing from our image (as these dark regions emit very few photons with respect to the warmer photosphere, and therefore very few circularly polarized photons as well). Another potential source of concern is the incompleteness of the reconstructed images when the associated data set features relatively large gaps in rotational phase coverage; as emphasized in Section 2.2 already, brightness and radial field maps may indeed easily miss low-latitude spots that have only been observed close to the approaching and receding stellar limbs, those very features azimuthal field maps are especially sensitive to. One must therefore be very cautious when interpreting potential differences between brightness and magnetic field maps obtained from incomplete data sets.

It nevertheless seems clear already that a significant fraction of the magnetic flux (and in particular the radial field region at phase 0.62, reasonably covered in both Stokes *I* and *V* data sets) comes from regions at photospheric temperature, as already suggested by Donati et al. (1997, 1999) and Donati & Cameron (1997).

3.3 1992 December

Fig. 4 displays the results corresponding to epoch 1992.94. Both radial and azimuthal field maps feature clear magnetic regions in which the local field strength often exceeds 1 kG. Note in particular that the polarity of azimuthal field regions is the same as what was observed at epochs 1990.9 and 1991.96, i.e. positive and negative at low and high latitudes respectively. The essential difference with the 1990.9 and 1991.96 magnetic images is that strong radial field regions are now present at the stellar surface, concentrating essentially at intermediate to high latitudes. As radial field spots tend to produce larger Stokes *V* signatures than azimuthal field ones (see Donati & Brown 1997), we believe that the absence of such radial field features at epoch 1990.9 and their progressive appearance in the following two maps are real, and cannot be attributed to an increased quality of the data set. Only weak meridional features are reconstructed at that epoch, most of them (and in particular low to intermediate latitude ones) being likely due to crosstalk from radial to meridional field orientations (Donati & Brown 1997). Note once more that ZDI detects preferentially the radial/meridional (respectively azimuthal) field features located close to (respectively between) phases of observations, as in all previous and following images for which only moderate phase coverage is available.

The brightness image reveals a large polar feature extending down to the equator at phase 0.47 and 0.85, along with a smaller appendage at phase 0.65. It is in good agreement with that published by Jankov & Donati (1995) obtained from an independent data set (involving a single spectral line and *BV* photometry), but with increased spatial resolution thanks to the higher spectral resolution (Donati et al. 1997), the S/N ratio enhancement provided by LSD and the short term monitoring of line profiles (see next paragraph). Although the raw temperature image reconstructed (from spectroscopic data only) by Vogt et al. (1998) at the same epoch shows some differences at low latitudes, their photometrically constrained thresholded version (which selects in principle only the most reliable surface features) repeats the basic features of our map quite well, with a clear elongation of the polar spot towards phase 0.5 and a low-latitude appendage around phase 0.85.

Note that significant evolution in the shape of both Stokes *I* and *V* profiles is detected on time-scales as short as a few per cent of the rotation cycle (and especially between phase 0.80 and 0.88, see lower panel of Fig. 4). It is important to realize that this short-term evolution of line profiles is indeed very helpful to constrain the imaging process further, as already emphasised by Donati & Brown (1997) in the particular case of magnetic imaging. We observe in particular that it can locally *enhance* spatial resolution at the stellar surface (as evidenced through the fine structures the code reconstructs within the low-latitude appendages of the polar spot in the brightness map for instance) through the *stereoscopic* viewing of the star it provides within each rotational phase block.

The lack of apparent spatial correlation between magnetic and brightness features is even more obvious than at epoch 1991.96, with some of the main magnetic features (such as the azimuthal field one at phase 0.35) found to be at photospheric temperature. Note that incomplete phase coverage cannot be invoked to explain this discrepancy (see Sections 2.2 and 3.2) as the brightness image derived by Jankov & Donati (1995) from a much denser data set does not include either any major spot that can be associated with the counterclockwise azimuthal field region we reconstruct at phase 0.35.

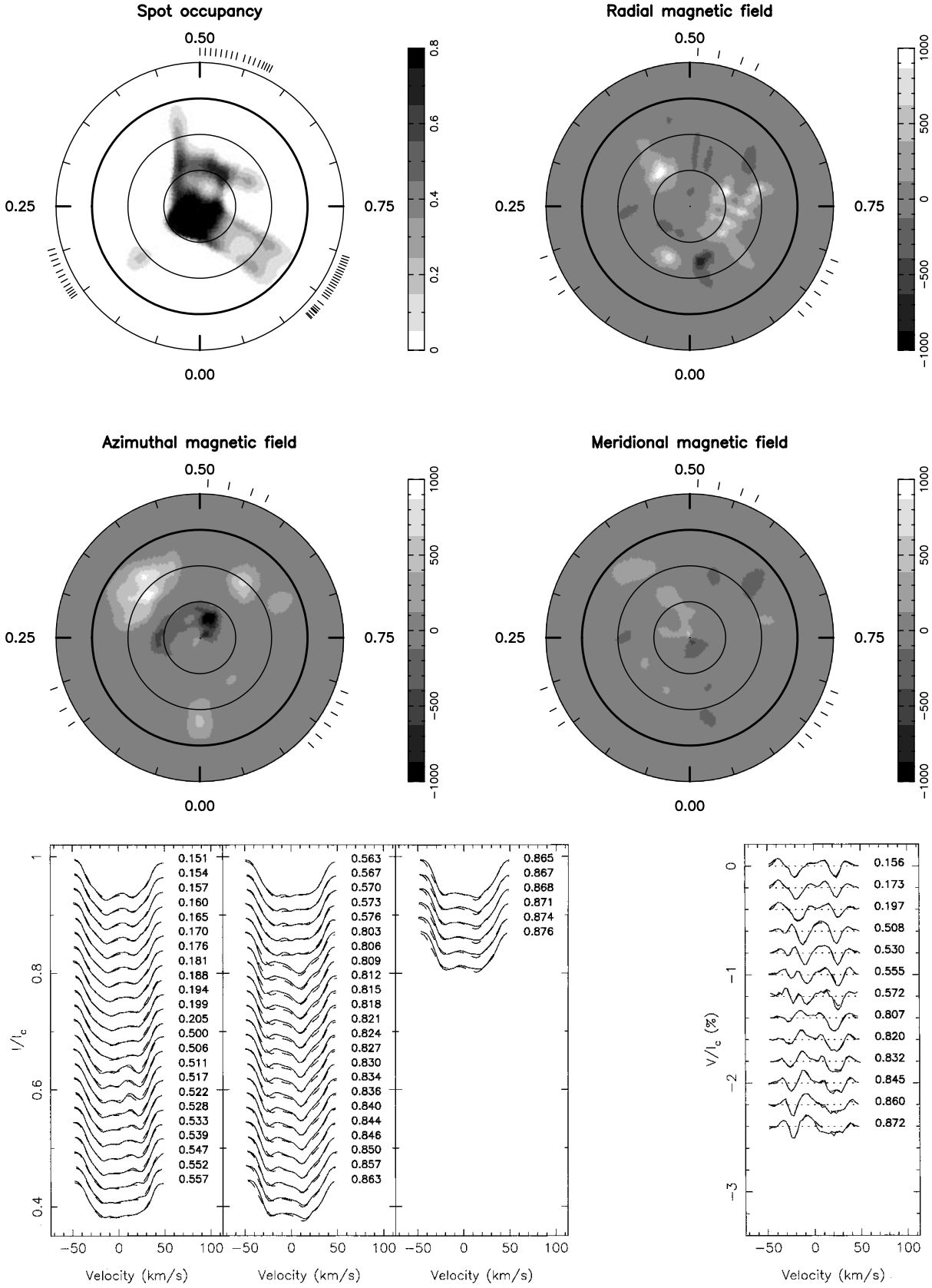

Figure 4. Same as Fig. 3 for HR 1099 at epoch 1992.94.

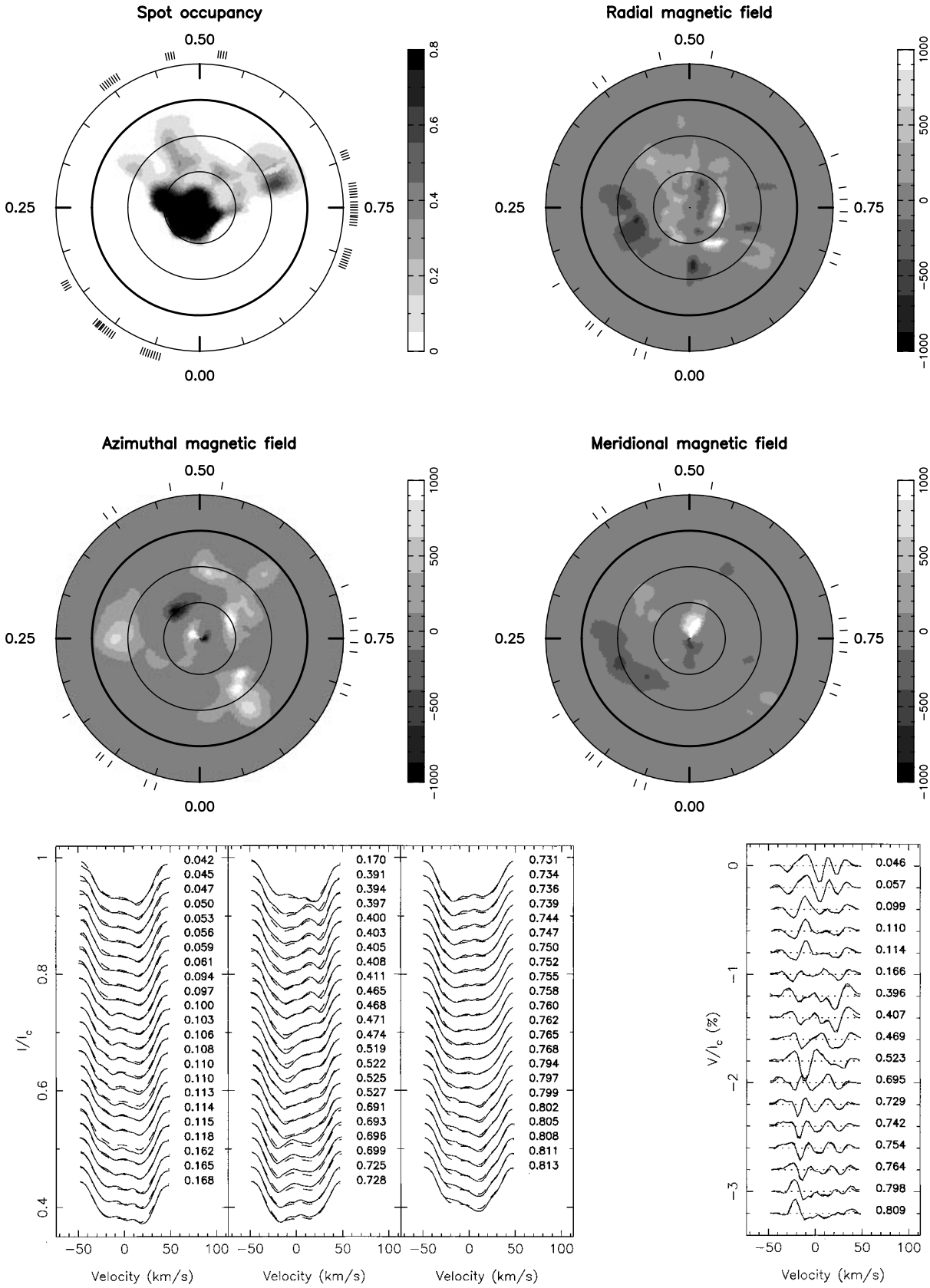

Figure 5. Same as Fig. 3 for HR 1099 at epoch 1993.99.

3.4 1993 December

The magnetic topology of HR 1099 at epoch 1993.99 (see Fig. 5) shows several new characteristics with respect to the previous ones.[2] The first interesting point is that a bipolar spot pair is reconstructed right at the rotational pole, both in the azimuthal and meridional field images. (Note that high latitude meridional field features cannot be attributed to crosstalk problems, as demonstrated in Donati & Brown 1997.) It is important to understand that these two bipolar groups actually form a single larger elongated magnetic region (directed and offcentred towards phase 0.53) in which the field is roughly horizontal and *homogeneously oriented* (pointing towards phase 0.03); the splitting of this feature into an azimuthal and a meridional field subcomponent as well as the bipolar aspect of these subcomponents are indeed only visual artifacts owing to the fact that the pole is a singular point in spherical coordinates. This single feature probably also connects with the spot of clockwise azimuthal field at phase 0.38, forming an incomplete ring of mainly clockwise azimuthal field which has suffered some kind of off-centring (by an amount of about 10–20°) towards phase 0.25.

The remaining (counterclockwise) azimuthal field regions are distributed all the way from latitude 20° (at phase 0.25) up to latitude 60° (at phase 0.68) rather than being confined at a latitude of 30° or so like at previous epochs. It also suggests that they all belong to a parent ring of counterclockwise azimuthal field, slightly tilted towards phase 0.25 by typically 10–20°. Moreover, the similar offcentring of these two low-/high-latitude rings of counterclockwise/clockwise azimuthal field suggests that both belong to the same large-scale structure (see Section 5.1 for further discussion).

Strong radial field features are also present at intermediate to high latitudes in this image. It even looks as if field vectors preferentially emerge from the star at a latitude of about 60°, while they tend to penetrate the photosphere at a latitude of about 30° and close to the rotational pole. Note that it may also have been the case at epoch 1992.94, although the correlation looks looser at that time. Strangely enough, the radial field distribution does not seem to suffer the off-centring that both azimuthal field rings clearly exhibit. All meridional field features apart from the bipolar group at rotational pole (and especially that at phase 0.20 and latitude 30°) essentially mimic radial field regions and are therefore attributable to crosstalk problems.

Our brightness image is similar to those we reconstructed at epochs 1991.96 and 1992.94, in the sense that it features once more a large spot close to the rotational pole with several low-latitude appendages, whose location on the stellar surface (at phase 0.30, 0.70 and 0.45 in this particular case) does not seem to show any obvious spatial correlation with magnetic features. No contemporaneous brightness image is available in the literature for potential comparisons with ours (as also the case for the next two following epochs).

3.5 1995 December

The HR 1099 maps we reconstruct at epoch 1995.94 (see Fig. 6) basically repeat the points we emphasized for epoch 1993.99. In particular, the azimuthal field image clearly demonstrates that low-latitude spots of counterclockwise field all belong to a parent ring-like structure encircling the star at latitude 30° or so. The high-latitude ring of clockwise field (most conspicuous at epoch 1990.9) is also very clear (and slightly off-centred towards phase 0.30, as evidenced by the strong bipolar group of meridional field spots detected at the rotational pole, see Section 3.4) in this new map. Strong radial field spots of positive polarity are found to gather at a latitude of about 60° while weaker negative polarity ones seem to concentrate preferentially at a latitude of about 30°, just as they used to do in the 1993.99 magnetic image.

The brightness image we obtain shows a polar spot significantly off-centred towards phase 0.30, with at least two latitude appendages at phase 0.0 and 0.8. It is interesting to note that the strong high-latitude ring of clockwise azimuthal field (defined by the high-latitude features in both azimuthal and meridional field maps) closely follows the high-latitude boundary of the polar spot and was probably doing so in previous maps (especially at epoch 1992.94 and 1993.99) already. Although it is not quite clear why the low-latitude boundary of the polar spot shows no obvious counterpart in the magnetic map, the above mentioned association is probably the best evidence we can find of potential spatial correlation between brightness and magnetic features. It is nonetheless obvious that any such correlation is much weaker in HR 1099 (where low-latitude regions of strong counterclockwise azimuthal field are very often found far away from all reconstructed cool spots) than in the Sun. The case of the strong counterclockwise azimuthal field feature reconstructed at phase 0.27 and for which no brightness counterpart can be identified (even though the Stokes *I* data set is reasonably well sampled at these rotational phases) is a particularly good illustration of this point.

3.6 1996 December

The last image of the series (shown in Fig. 7) corresponds to epoch 1996.99. Although the azimuthal field map is structurally similar to those observed at previous epochs (with low-/high-latitude regions of counterclockwise/clockwise field respectively), its overall intensity is slightly weaker. The radial field component on the other hand does not seem to undergo any noticeable change in intensity, with strong fields emerging from the photosphere around latitude 60° or so. The correlation between latitude and radial field polarity (positive at latitude 60° and negative at low and polar latitudes) suggested from previous magnetic maps is strengthened in this new image. A point worth noting is that relatively strong (i.e. –800 G) radial fields are detected very close to the rotational pole at this epoch.

The brightness image exhibits a high-contrast high-latitude feature off-centred towards phase 0.43 with respect to the rotational pole. As for the previous epochs, the only noticeable spatial correlation between magnetic and brightness maps is that the high-latitude boundary of the brightness polar feature coincides with the high-latitude off-centred ring of clockwise azimuthal field (witnessed through the azimuthal/meridional field features we detect at latitudes 60° and more).

4 THE YOUNG DWARF LQ HYA

4.1 Preparing the data set

The data set for LQ Hya is much easier to prepare, thanks to the fact that this star is single. We simply recentre all line profiles by selecting the radial velocity that minimizes the information content of the reconstructed image (yielding a value of 8.6 ± 0.5 km s^{-1}).

[2] Note that the maps of Fig. 5 supersede the preliminary versions published by Donati (1996a,b) for which field polarities or/and field strength scales were wrong.

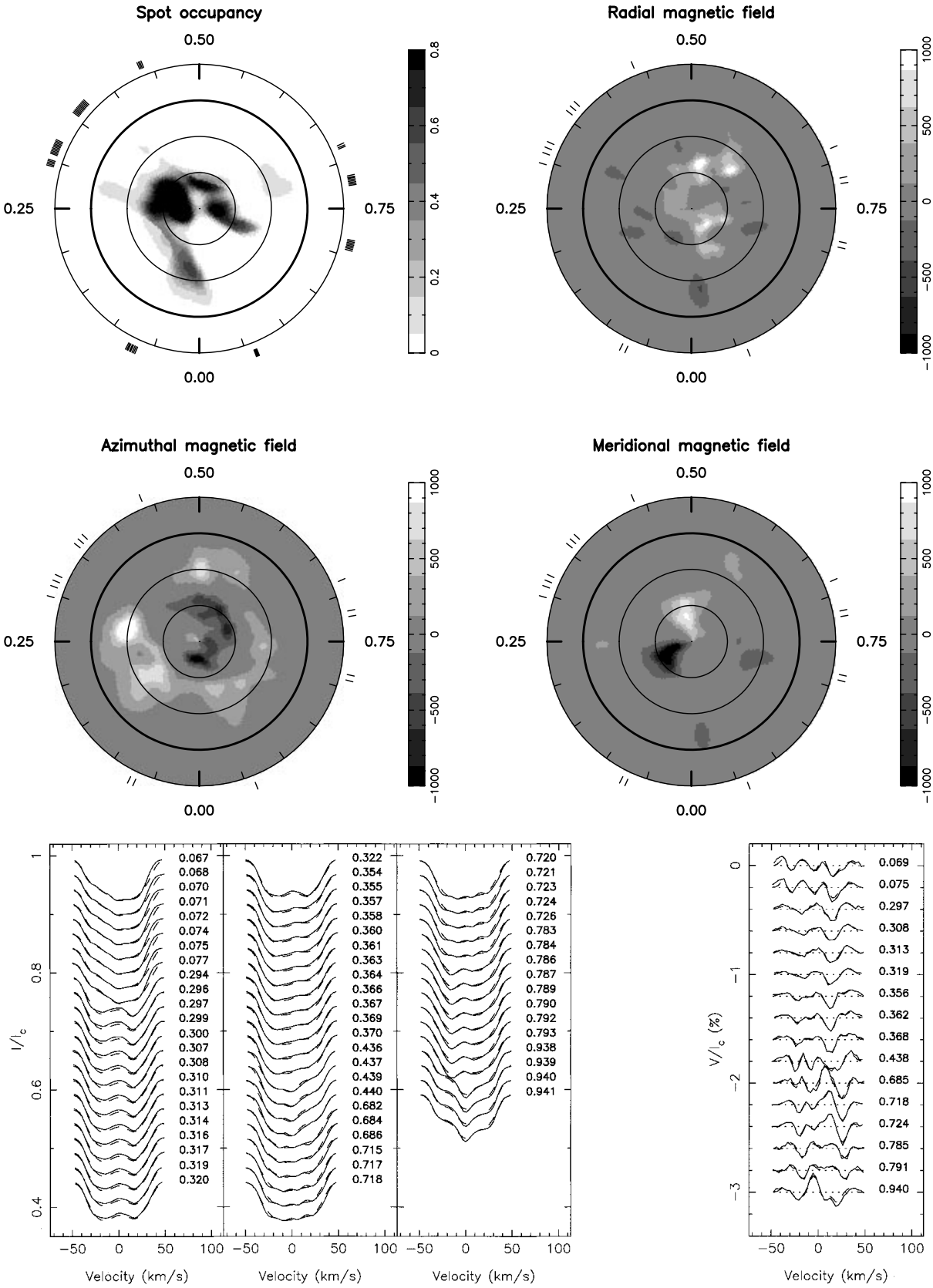

Figure 6. Same as Fig. 3 for HR 1099 at epoch 1995.94.

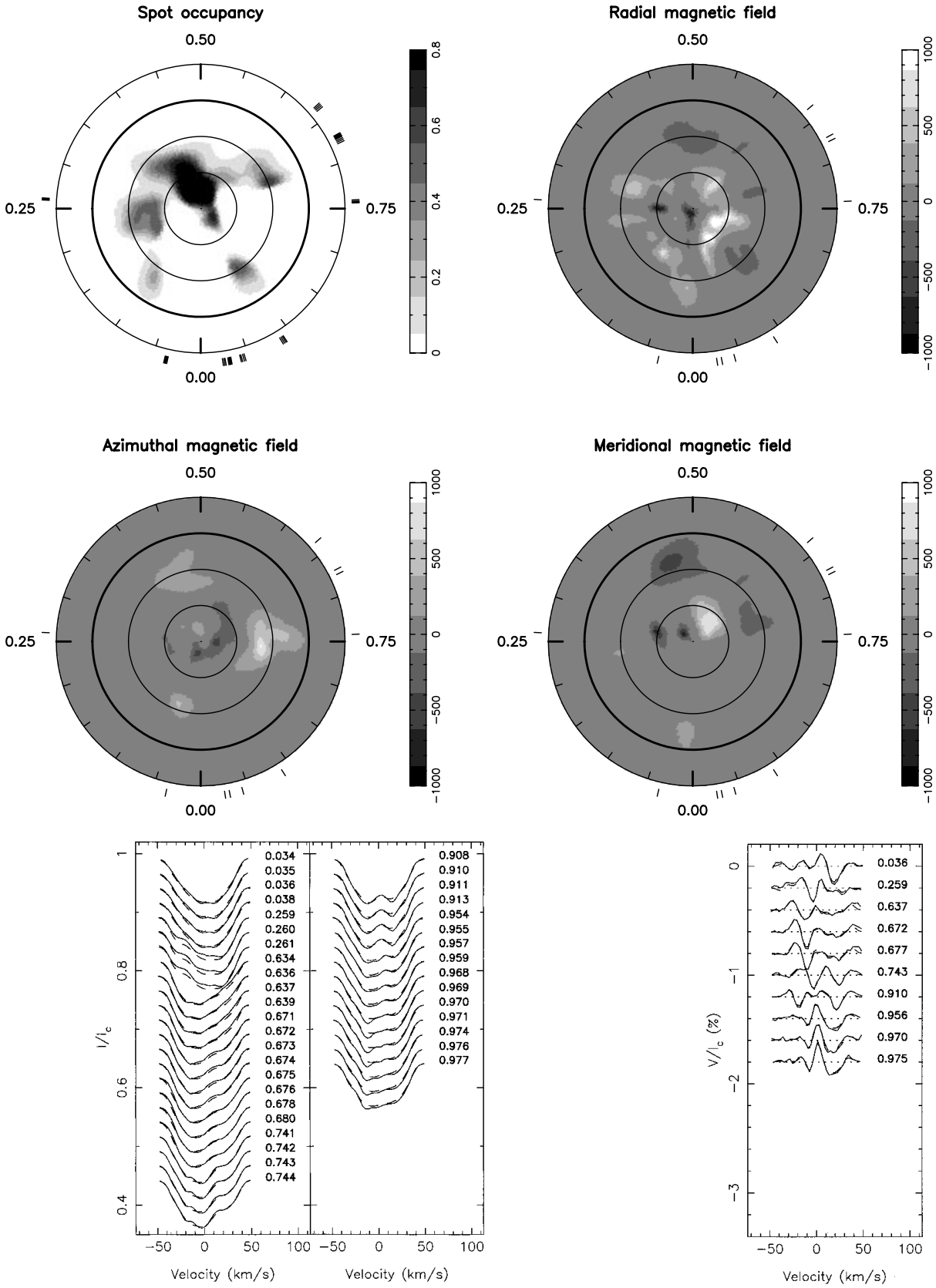

Figure 7. Same as Fig. 3 for HR 1099 at epoch 1996.99.

We can obtain the inclination angle i and the projected rotational velocity $v \sin i$ with the same method, and derive most likely estimates (averaged over the different observing epochs) of $i = 55 \pm 5°$ and $v \sin i = 26.5 \pm 0.5$ km s^{-1}.

Using the new *Hipparcos* (Perryman et al. 1997) parallax yielding a distance of 18.35 ± 0.35 pc for LQ Hya, we can obtain a second independent estimate of the inclination angle (just as we did for HR 1099, see Section 3.1.2). Using $m_V = 7.6 \pm 0.1$ as the unspotted visual brightness, and 5000 ± 100 K as the effective temperature (implying a bolometric correction of -0.40 ± 0.05, Kurucz 1993), we obtain a bolometric magnitude of 5.9 ± 0.2 and a radius of 0.8 ± 0.1 $R_\odot$. Independently, the measured period (1.606 d, Strassmeier et al. 1993) and $v \sin i$ (see previous paragraph) yield a line-of-sight projected radius of 0.84 ± 0.02 $R_\odot$. Both estimates can only be made compatible for inclination angles larger than 65°.

The value we finally chose (60°) represents a compromise between the two constraints above. Note that, as for HR 1099, potential errors of $\pm 10°$ on the inclination angle produce only very small differences in the reconstructed images.

All LQ Hya images presented below correspond to fits at relative noise levels of 0.12 per cent to 0.17 per cent (S/N ratio ranging from 600 to 800 depending on the epoch) for Stokes I profiles, and to unit reduced χ^2 levels for Stokes V profiles. While the total spottedness and mean field strength the code reconstructs are respectively equal to 5 per cent and 90 G on average (i.e. about twice smaller than those we find for HR 1099), the brightness and magnetic filling factors however are respectively equal to 8 and 16 per cent respectively (i.e. very similar to those obtained for HR 1099).

All rotational phases listed below are computed with the ephemeris of Strassmeier et al. (1993). The small time intervals over which each data set was collected ensures that potential internal phase inconsistency due to yearly variations in photometric period (i.e. to surface differential rotation, e.g. Strassmeier et al. 1997) is always smaller than 1 per cent of the rotational cycle.

4.2 1991 December

The LQ Hya data set for epoch 1991.96 is very fragmentary, with observations gathering essentially in two main phase groups. The associated maps (see Fig. 8) must therefore be taken with caution. Note in particular that most points on the stellar surface located between phase 0.86 and 0.97 have not been observed at all.

As no additional crosstalk from radial/meridional to azimuthal field is expected when inverting sparse data sets (Donati & Brown 1997), the maps of Fig. 8 suggest at least that clockwise azimuthal fields stronger than 200 G must be present at the surface of LQ Hya to explain the observed rotational modulation of Stokes V profiles. Although very rough, the corresponding brightness map also indicates the presence of at least two groups of dark features (at phase 0.28 and 0.70) whose signatures in Stokes I profiles are obvious.

4.3 1992 December

Although still fragmentary, observations collected at epoch 1992.94 are numerous enough to ensure that all points on the stellar surface located above the equator were observed at least once. The corresponding magnetic map (shown in Fig. 9) confirms in particular what the previous section suggested, i.e. that clockwise azimuthal field regions are present at the surface of LQ Hya. It also indicates that all features in the azimuthal field map have the same polarity, conversely to what was reported for HR 1099 where low and high latitudes are associated with different azimuthal field polarities (see Section 3). Several radial field regions (and in particular a major negative polarity one in which the field reaches about 350 G) are also reconstructed at this epoch. Note that this image is a good illustration of the fact that ZDI detects preferentially radial (respectively azimuthal) field regions located close to (respectively between) phases of observation when only moderate phase coverage is available, as predicted in Section 2.2 and observed on HR 1099.

The brightness image features several obvious low-latitude spots (at phase 0.0, 0.49, 0.60 and 0.75 in particular) whose impact on the recorded Stokes I profiles is quite clear. Worth noting is the fact that radial/azimuthal field features at phase 0.50, 0.60 and 0.80 are found to coincide rather well with (or at least to be located very close to) dark counterparts in the brightness image. This may suggest that the spatial correlation between magnetic and brightness features is slightly stronger for LQ Hya than for HR 1099, although definitely not as tight as for the Sun.

4.4 1993 December

At epoch 1993.99, observations are significantly more numerous and evenly spread throughout the rotational cycle compared to the previous two runs. The corresponding magnetic map is shown in Fig. 10.[3] It demonstrates in particular that the field is preferentially clockwise oriented within all azimuthal field regions of LQ Hya, as already suggested from the previous two maps. It also establishes that radial field preferentially points towards the star (rather than away from it), and was probably doing so at epoch 1992.94 already. There is not much to conclude from the fact that the reconstructed magnetic map does not show any low-latitude meridional field regions, since stars with high inclination angles are not sensitive to this kind of magnetic features (Donati & Brown 1997). The very weak meridional field feature reconstructed close to the rotational pole suggests however that most magnetic field concentrates in the two other (i.e. radial and azimuthal) field components on LQ Hya.

The corresponding brightness map is reasonably well constrained. It features in particular a dark region close to the rotational pole and extending all the way down to the equator towards phase 0.40, as well as a few distinct and isolated low-latitude spots (at phase 0.24, 0.57, 0.87 and 0.99) whose potential association with magnetic spots is not obvious.

4.5 1995 December

Most LQ Hya observations collected at epoch 1995.94 gather around two main rotational phases shifted by about half a rotation cycle. The reconstructed maps (see Fig. 11) must therefore be considered with caution, even though all points on the stellar surface above the equator have been observed at least once.

The azimuthal field map features several spots of rather intense clockwise field at both low and high latitudes. Similarly, the radial field map essentially shows regions of downward pointing field, whose intensity reaches up to 900 G. Although LQ Hya also hosts a few regions of weaker counterclockwise azimuthal and outward pointing radial field close to the equator, negative polarity regions clearly dominate both maps at all latitudes, further strengthening the conclusions reached at previous epochs.

[3] Note that the maps of Fig. 10 supersede the preliminary ones of Donati (1996b) for which the field strength scale was wrong.

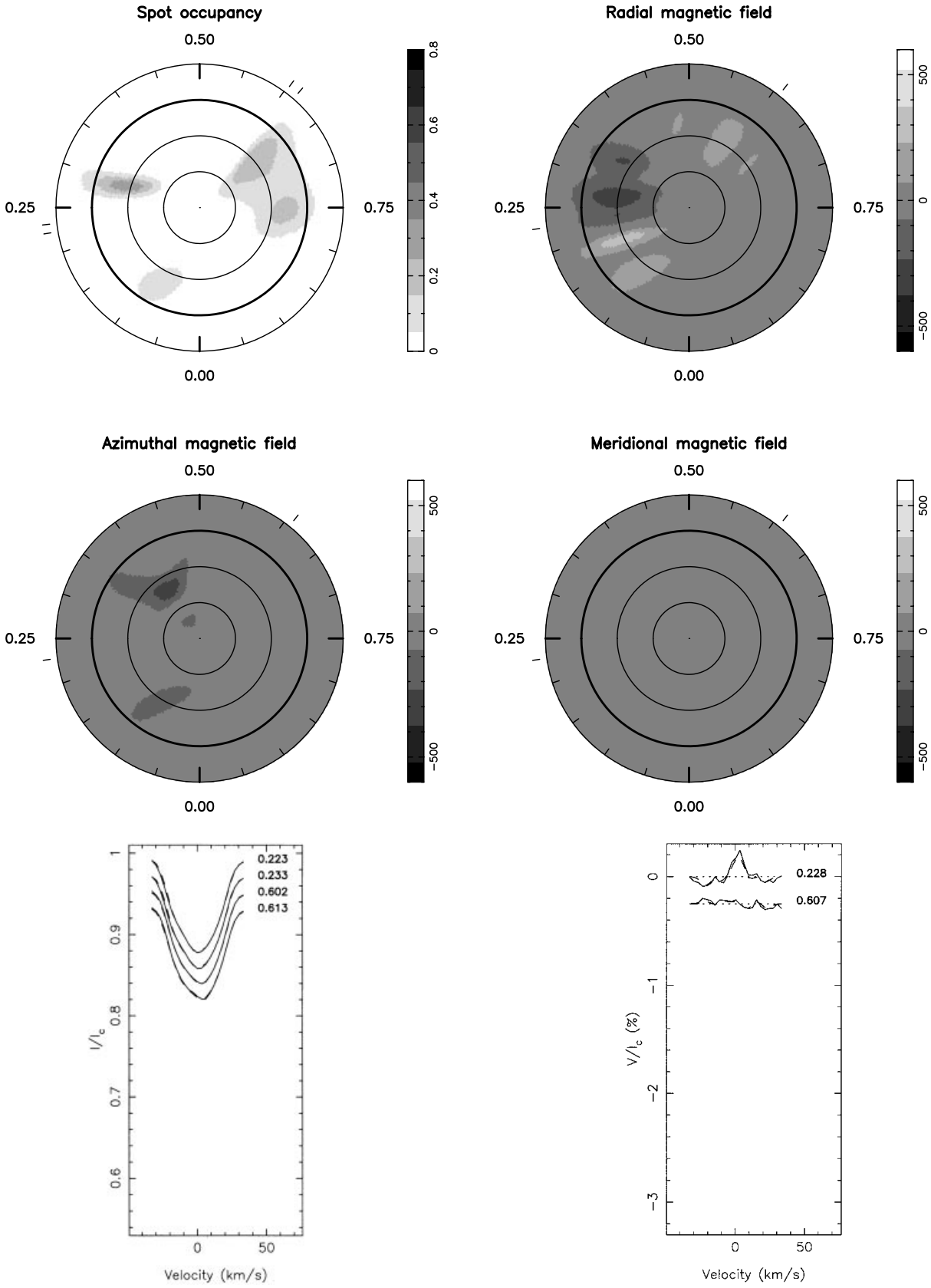

Figure 8. Same as Fig. 3 for LQ Hya at epoch 1991.96. Note that the grey-scale table only ranges from −600 G to 600 G now.

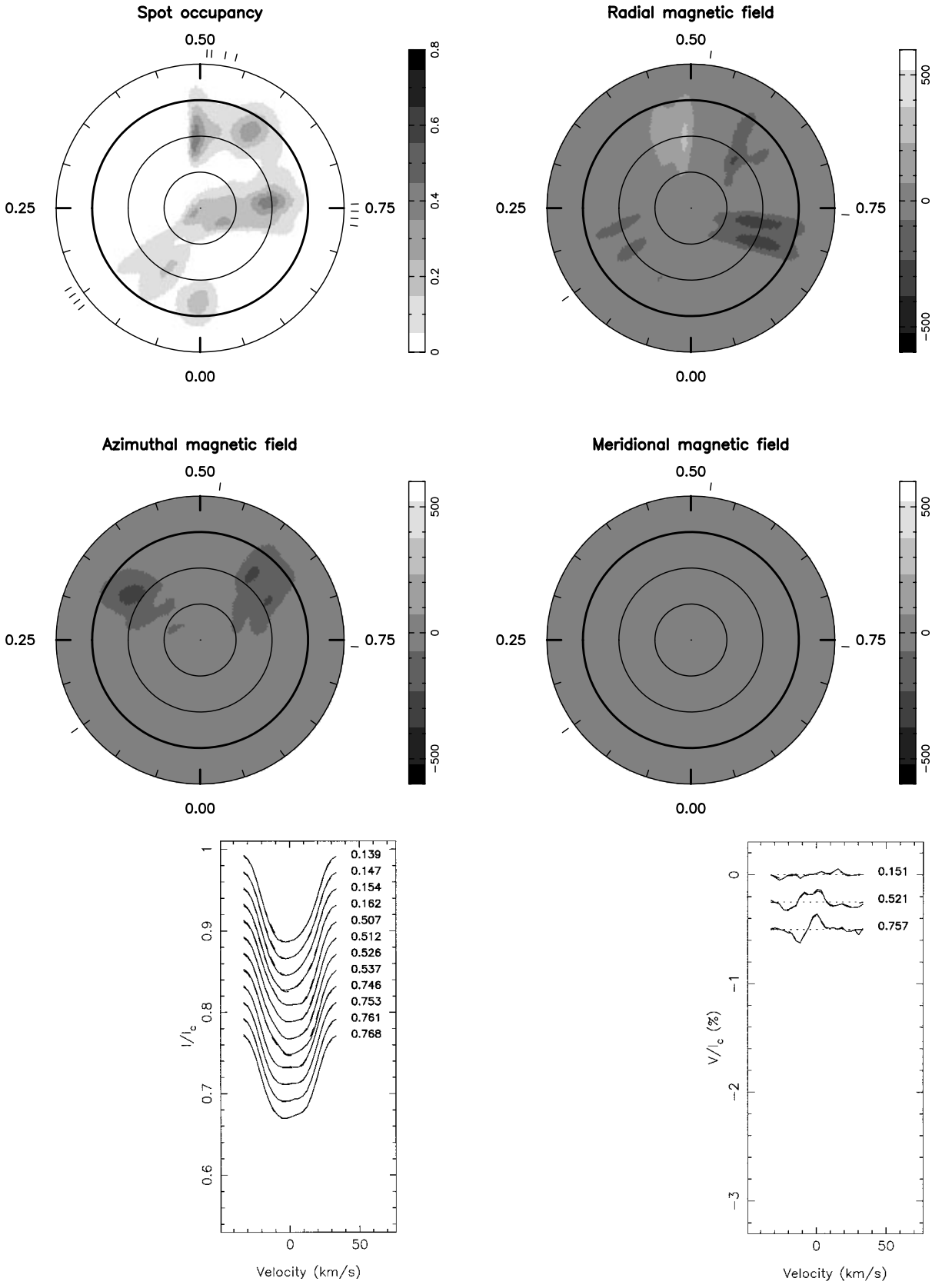

Figure 9. Same as Fig. 8 for LQ Hya at epoch 1992.94.

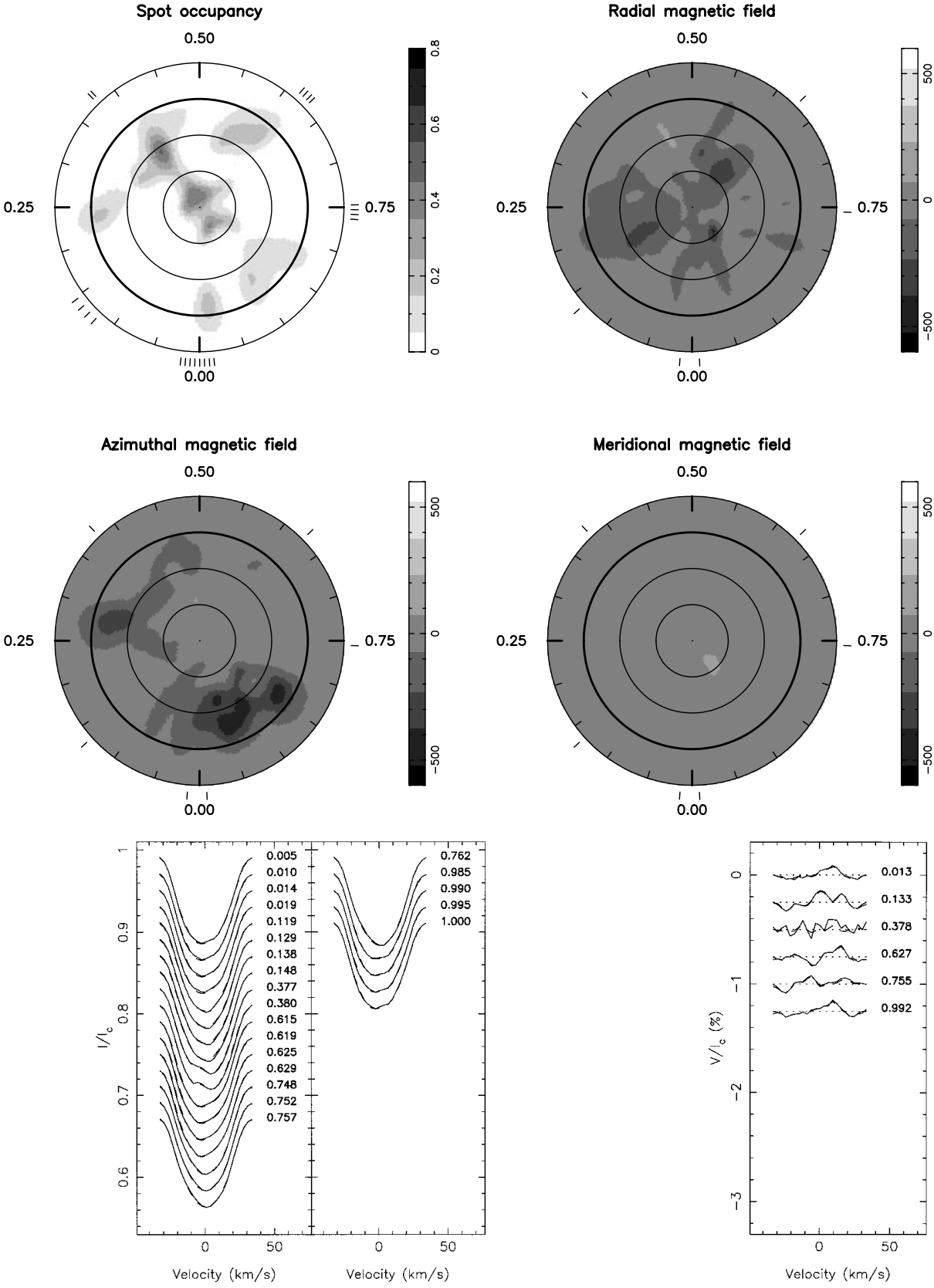

Figure 10. Same as Fig. 8 for LQ Hya at epoch 1993.99.

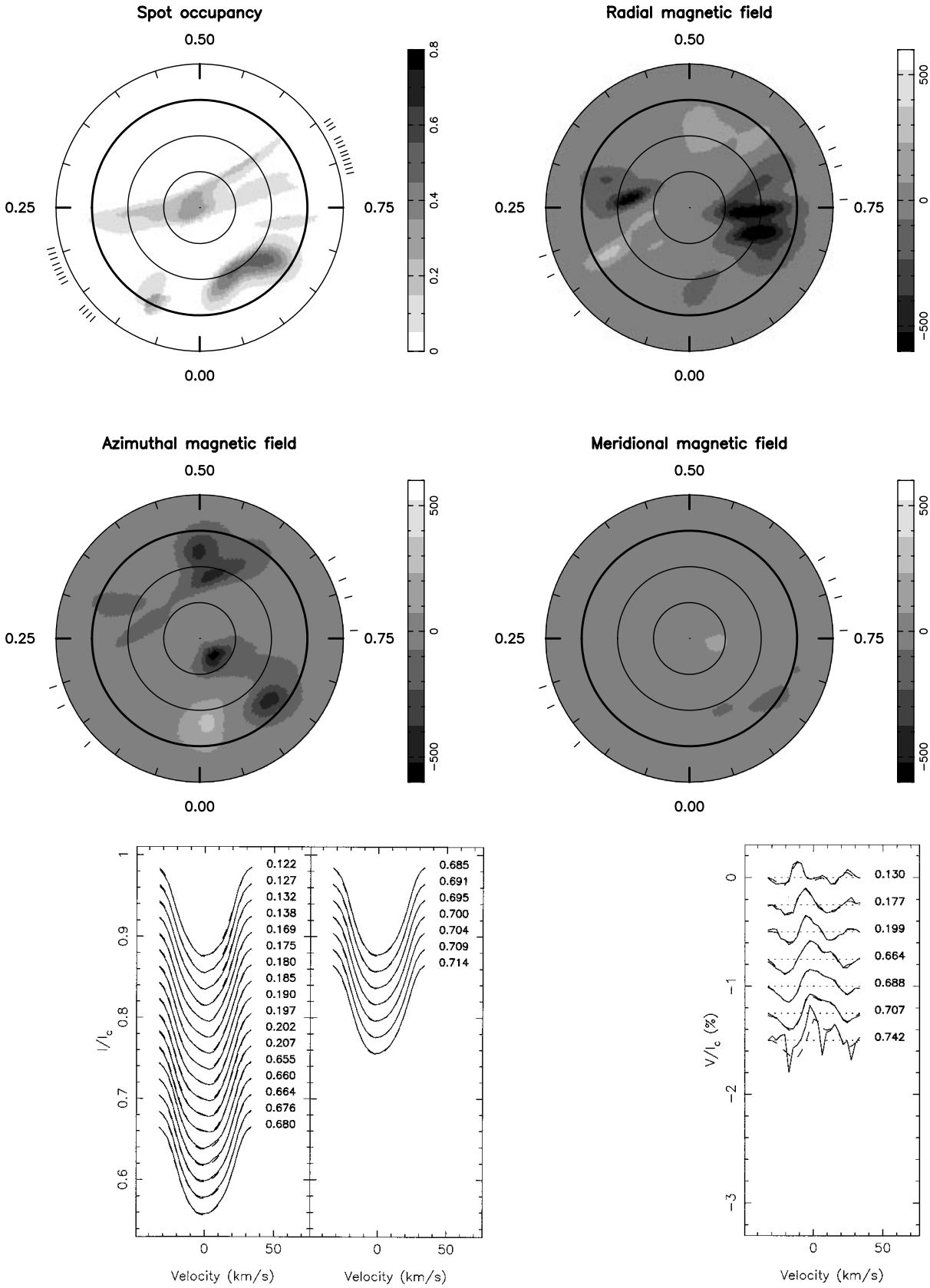

Figure 11. Same as Fig. 8 for LQ Hya at epoch 1995.94.

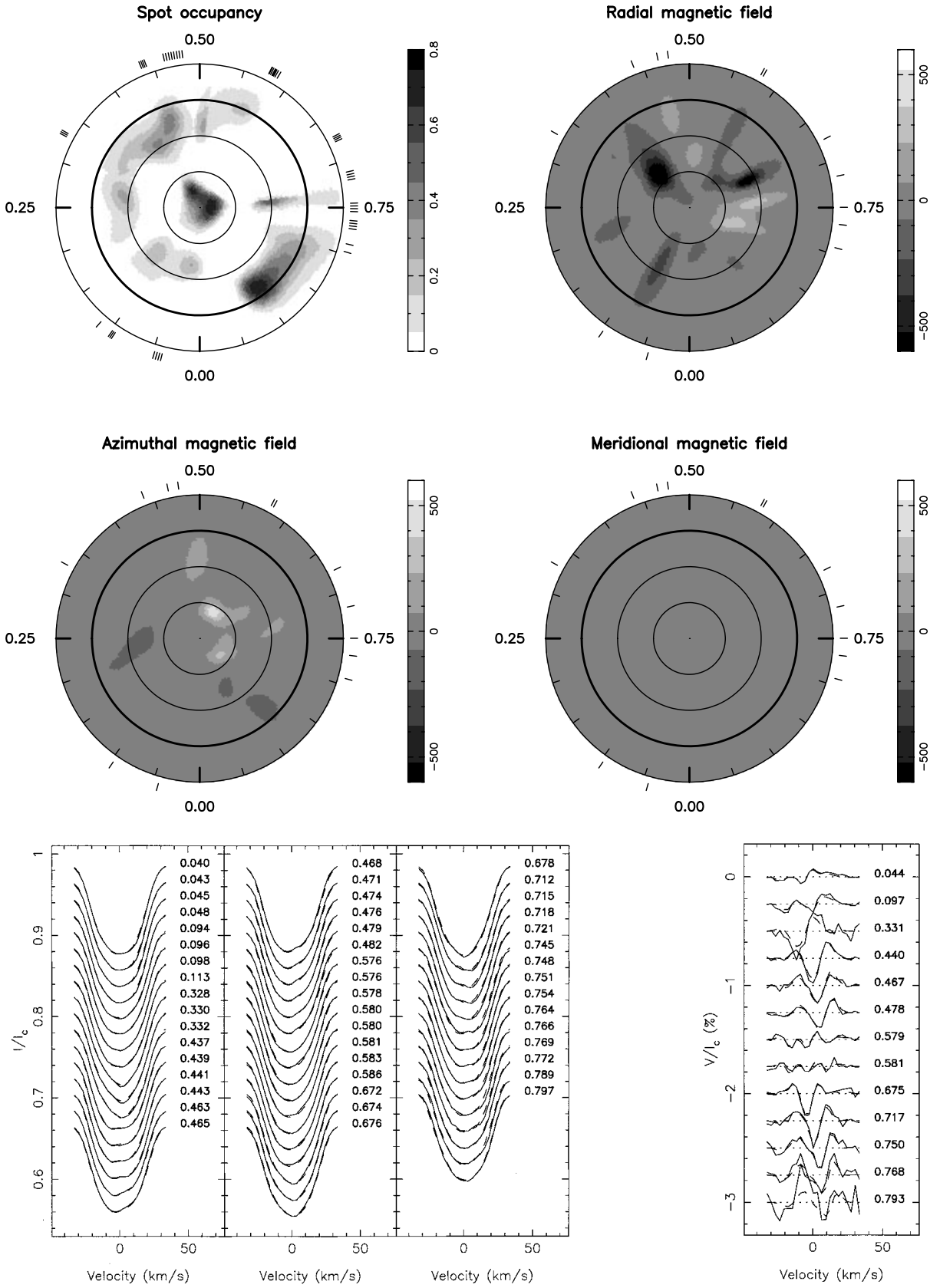

Figure 12. Same as Fig. 8 for LQ Hya at epoch 1996.99.

The brightness map features a dark region passing through the rotational pole and extending all the way down to the equator at phases 0.23 and 0.65–0.70. Its elongated shape is mostly a result of the sparse rotational phase sampling of the corresponding data set. Another low-latitude dark spot is also present at the surface of LQ Hya at this epoch at phase 0.80 (generating the depressions observed in the red/blue wings of Stokes *I* profiles at rotational phases 0.12/0.65 respectively).

4.6 1996 December

The 1996.99 LQ Hya data set is the most complete one of the whole series, making the corresponding maps (see Fig. 12) very well constrained and reliable. The azimuthal field image features essentially two high-latitude spots of counterclockwise field, plus several other weak low-latitude ones. Being now dominated by positive polarity field regions, this new map is noticeably different from the previous one and indicates that the magnetic topology of LQ Hya has undergone some structural modification between epochs 1995.94 and 1996.99. On the other hand, the radial field map shares obvious similarities with that at epoch 1995.94, featuring essentially several negative polarity regions (in which the field reaches about 800 G), with a few much weaker positive polarity spots. No discernible meridional field feature is detected.

The brightness image is quite complex, including a dark asymmetric region located close to the rotational pole, as well as several (up to eight) low-latitude regions unevenly distributed around the star. It is worth noting that one magnetic spot at least (the negative polarity radial field feature at phase 0.68) has no obvious counterpart in the brightness image even though observations are quite dense at this particular phase; it strengthens the conclusion that magnetic features do not necessarily coincide with brightness ones, even for LQ Hya. Note that this image is very reminiscent of those obtained for the other similarly young dwarf AB Dor (Donati & Cameron 1997; Donati et al. 1999), if we keep in mind that the lower rotation rate of LQ Hya (about 3.1 times smaller than that of AB Dor) implies lower spatial resolution for the corresponding Doppler image.

5 DISCUSSION

5.1 Topologies of non-solar dynamo magnetic field structures

As pointed out throughout Sections 3 and 4, all magnetic images we reconstruct for HR 1099 and LQ Hya show that a significant (and even sometimes dominant) fraction of the overall magnetic field of HR 1099 and LQ Hya is stored in azimuthal field regions. We stress once more that these azimuthal field regions are *not* artifacts of the reconstruction process. Simulations do indeed demonstrate that no crosstalk is expected between radial/meridional field and azimuthal field maps even when only moderate to poor phase coverage is available (Donati & Brown 1997), implying that the presence of the azimuthal field regions we detected is definitely required at the surface of both stars for explaining the observed rotational modulation of Stokes *V* profiles down to photon noise level. Similar conclusions were also reached in the case of another cool active star, the young ultra-fast rotator AB Dor for which extremely dense Stokes *V* data sets could be recorded (Donati & Cameron 1997; Donati et al. 1999). The fact that these azimuthal field regions are often reconstructed *between* (rather than in conjunction with) phases of observations (especially when phase coverage is moderate) is perfectly normal and only illustrates that ZDI is mostly sensitive to such features when they are about 0.2 rotation cycle away from their phase of meridian crossing (see Section 2.2).

Although the actual distribution of these magnetic regions changes beyond recognition from epoch to epoch, we observe that their *polarities* are essentially *longitude independent at a given latitude* (e.g. counterclockwise and clockwise field at low and high latitudes respectively for HR 1099). Moreover, this latitudinal pattern of azimuthal field polarities is roughly constant on time-scales of a few years (e.g. all azimuthal field maps of HR 1099 available to date show counterclockwise and clockwise field rings at low and high latitudes respectively). Our observations therefore suggest that these regions are not due to random manifestations of magnetoconvection within the stellar photosphere, but actually witness the presence of a large-scale roughly axisymmetric toroidal field structure, stable on time-scales of several years. We speculate that this large-scale structure is that generated by dynamo mechanisms, like that of the Sun for instance except for the fact that the one we detect in HR 1099 and LQ Hya is directly visible at photospheric level. The results of Sections 3.4 and 3.5 suggest that this large scale toroidal structure can sometimes be slightly tilted with respect to the rotational pole, by angles of 10°–20° typically. This tilt of the toroidal structure is also reflected in the brightness distribution.

Although slightly less obvious from individual images, similar conclusions apply for the radial field maps of HR 1099 (showing a tendency for positive radial fields at intermediate to high latitudes and negative radial fields at low and circumpolar latitudes) and LQ Hya (for which radial field are essentially negative at all latitudes). Note in particular that these radial field topologies are clearly different from that of the young dwarf AB Dor (Donati & Cameron 1997; Donati et al. 1999), for which the polarities of major radial field features does not seem to correlate well with latitude nor to repeat from one year to the next. Following the idea of the previous paragraph, we speculate that the latitudinal polarity pattern of radial fields we observe for HR 1099 and LQ Hya witnesses the poloidal component of the dynamo-induced large-scale field structure, also visible at photospheric level. For some yet unknown reason, this structure does not seem to reflect the angular tilt visible in both large-scale toroidal structure and brightness distribution.

The time-averaged latitudinal dependence of the observed azimuthal and radial field distributions is shown in Fig. 13. Note that it is not possible to recover azimuthal and radial field distributions in the other hemisphere, as Stokes *V* profiles are only very weakly sensitive to features located at negative latitudes. The observed polarity pattern nevertheless suggests that the axisymmetric component of the radial field distribution (and therefore presumably the parent large-scale poloidal field structure as well) resembles a spherical harmonic mode with a ℓ degree equal to 5 or more, while that of LQ Hya is closer to a simple dipole. The amplitude of these harmonic modes are several hundred G, i.e. at least two orders of magnitude stronger than in the Sun.

The Stokes *V* signatures we detect within the lines of the secondary star of HR 1099 may be an independent suggestion that poloidal fields at the surface of the K1 subgiant are rather strong. The relatively simple (i.e. roughly antisymmetric) shape of the Zeeman signature associated with the spectral lines of the G5 star (see Fig. 2), as well as its weak dependence on rotational phase and epoch (see Section 3.1.1) are indeed indications that the associated magnetic field must be grossly homogeneous, like for

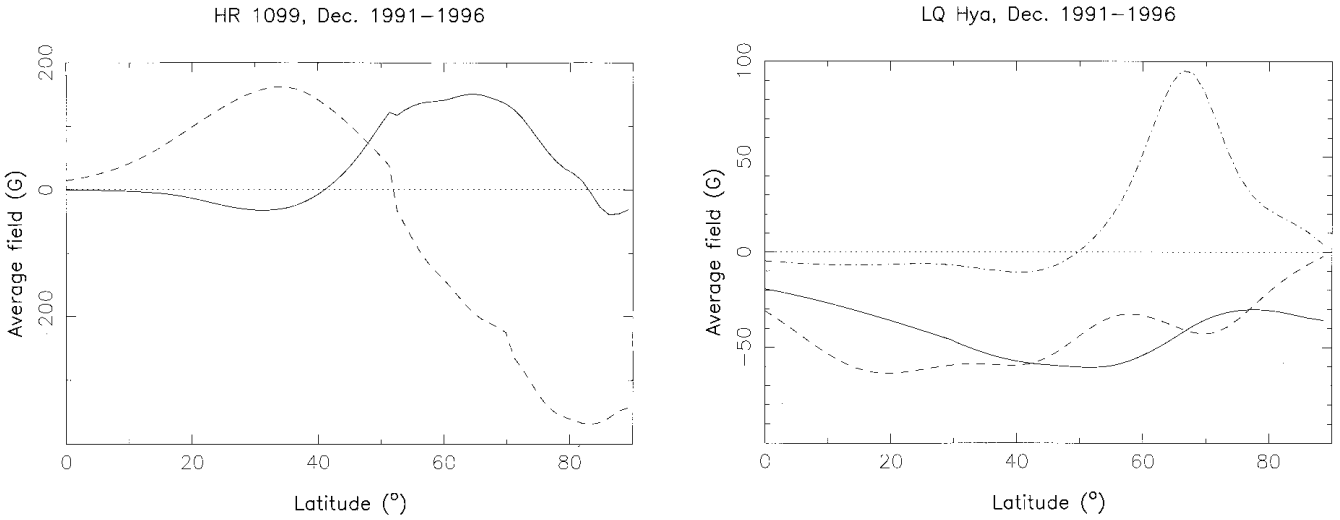

Figure 13. Latitudinal pattern of radial (solid line) and azimuthal (dashed line) magnetic field distributions of HR 1099 (left panel) and LQ Hya (right panel), once averaged over longitude and time. Note that the LQ Hya 1996 December latitudinal pattern of azimuthal fields (dot–dash line) was not included in the time average. Meridional fields at latitudes higher than about 50° as well as azimuthal field at latitudes higher than 70° were counted as clockwise azimuthal field for HR 1099, according to the conclusions of Section 3.4. Meridional fields at latitudes lower than about 50° was counted as radial field for both stars, according to the conclusions of Donati & Brown (1997).

instance the large-scale poloidal structure of the K1 subgiant at the level of the orbit of the secondary star. On the other hand, the field topology the G5 star likely hosts (as a rapidly rotating solar-type star) is probably too complex to explain the Stokes V profile of Fig. 2, as it would generate Zeeman signatures featuring several (i.e. at least two) sign switches throughout the profile width and exhibiting strong rotational modulation, even for a $v \sin i$ as low as 12 km s^{-1}. In this context, the 10-G longitudinal field associated with this Zeeman signature translates into a polar field of 200 G (for a dipolar structure) or more (for higher orders of the spherical harmonics expansion), in good agreement with what we obtain from the magnetic images of the K1 subgiant (see Fig. 13).

We already have some evidence that the large-scale azimuthal and radial field structures vary slowly with time. Radial field regions (absent at epoch 1990.9, Donati et al. 1992b) have progressively appeared at the surface of HR 1099 while azimuthal fields remained fairly strong until 1996.99, when they may have started to decline (although this needs confirmation from future observations). Similarly, regions of counterclockwise azimuthal field have recently appeared at high latitudes on LQ Hya at epoch 1996.99 (see Figs 12 and 13), while radial field features remained roughly as strong. We speculate that these variations are linked to the long-term evolution of the parent large-scale poloidal and toroidal structures with time.

The only spatial correlation between magnetic and brightness regions we can report is that high-latitude azimuthal fields seem to coincide with the high-latitude boundary of the dark polar spot in HR 1099. Even though a weak correlation between low-latitude brightness and magnetic features may be present for LQ Hya, it is definitely far weaker than for the Sun, with strong magnetic features being clearly detected at photospheric temperature. This is in agreement with results previously reported for various RS CVn systems (from a colour analysis of Stokes V Zeeman signatures, Donati et al. 1997) and for the young dwarf AB Dor (Donati & Cameron 1997; Donati et al. 1999), but contradicts an earlier claim by Donati et al. (1992b) that magnetic regions on HR 1099 do coincide with dark features.

5.2 Implications for dynamo theories

The simple fact that stable azimuthal field regions are detected at photospheric level strongly indicates that the parent large-scale toroidal structure is not generated at the base of the convective zone, as in the Sun. It is very unlikely that these features represent the emergence of magnetic flux loops carried upwards either by granular convection or magnetic buoyancy (like those we see on the Sun, Lites et al. 1996), as they would only be stable on very short time-scales and would therefore not be observed repeatedly on successive rotational cycles (e.g. Donati & Cameron 1997; Donati et al. 1999). The obvious conclusion is thus that the parent toroidal magnetic field must be generated close to the stellar surface, and thus within the convective envelope itself. Another strong argument in favour of this conclusion is that rising flux tubes from a deep-seated magnetic structure located at the base of the convective zone are expected to emerge at high latitudes in rapidly rotating late-type stars (Schüssler 1996; DeLuca, Fan & Saar 1997). For instance, on a K1 subgiant like HR 1099 (with a convective zone as deep as 0.85 $R_\star$), flux tubes should all appear at latitudes larger than 60°, in strong contradiction with the field maps we reconstruct which very often show surface features at latitude 30° or so. Note that this second argument also applies for the reconstructed radial field maps, implying that some of the large-scale poloidal field at least is also generated close to the surface. Altogether, we consider that our observations provide strong evidence that poloidal and toroidal magnetic structures in these rapidly rotating active stars are generated within the convective zone, and therefore not throughout a solar-like overshoot-layer dynamo.

One of the arguments in favour of the solar overshoot-layer dynamo comes from the interpretation of helioseismological observations, which demonstrates that the radial gradient in angular velocity is roughly zero throughout the whole convective zone, except in a thin interface layer of convective overshoot between the radiative interior and convective envelope. This overshoot layer is therefore the only place that can turn poloidal fields into toroidal ones through large-scale rotational shear (the Ω process). Moreover,

it is probably the only place where magnetic fields can be retained on periods of time much longer than the duration of a solar cycle. However, it is not necessarily the place where poloidal magnetic fields are regenerated from toroidal ones by cyclonic turbulence or other non-mirror symmetric velocity fields (the α process). Observations of bipolar magnetic regions and calculations on rising buoyant magnetic flux from this overshoot layer actually suggest that the toroidal field it stores is much too strong (of the order of 10^5 G) to allow local convective turbulence and therefore efficient α process action (Parker 1993). The most recent dynamo models tend to concentrate the α effect (and the production of the poloidal field) somewhere else, either just above the overshoot layer (Parker 1993; MacGregor & Charbonneau 1997), or throughout the whole convective zone, or even very close to the stellar surface (e.g. Durney, De Young & Roxburgh 1993; Choudhuri, Schüssler & Dikpati 1995). Mechanisms such as magnetic diffusivity, turbulent pumping or large-scale meridional circulation are then invoked to couple α and Ω processes together and allow dynamo to operate in a cyclical manner. In particular, it is being increasingly realized that small-scale solar magnetic fields (and especially the intranetwork fields presumably generated within the bulk of the convective zone, Lin 1995) may contribute significantly to the large-scale solar dynamo field (Stenflo 1994; Lites et al. 1996).

In rapidly rotating stars like those we have observed to date (HR 1099, LQ Hya and AB Dor, rotating respectively 9, 16 and 51 times faster than the Sun), the situation is probably very different. As no internal differential rotation laws have been obtained yet through asteroseismology, we have to rely essentially on hydrodynamical models of the convective zone, like those of Kitchatinov & Rüdiger (1995) or Rüdiger et al. (1998). These papers show that for stars cooler or rotating faster than the Sun, the internal differential rotation pattern is very different from solar, with rotation rate being almost constant in cylindrical shells parallel to the rotation axis. It implies in particular that radial gradients of angular rotation should no longer be confined to the base of the convective zone as in the Sun, but distributed throughout the whole convective zone. Although such models (which predict that the difference in surface angular rotation between the equator and poles $d\Omega$ should decrease with rotation rate Ω as $\Omega^{-0.4}$) do not exactly reproduce direct surface differential rotation measurements in rapid rotators (which suggest that $d\Omega$ is essentially constant with Ω, Donati & Cameron 1997), they indicate at least that dynamos in rapidly rotating late-type stars are likely structurally different from solar, and bring some theoretical support to our conclusions that large toroidal field topologies must be generated within the convective envelope.

It therefore seems very likely that a significant fraction of the global field of rapidly rotating late-type stars is generated by a distributed dynamo (with both α and Ω effects located within the convective zone proper). Independent confirmation of this conclusion comes from the observation that poloidal and toroidal field components have similar strengths (see Fig. 13, in agreement with theoretical distributed dynamo models, e.g. Brandenburg et al. 1994), as opposed to the Sun where the observed poloidal field is several orders of magnitude smaller that the inferred toroidal component. Moreover, the strength of the large-scale poloidal field is of the order of a few hundred G, indicating that such distributed dynamos are very efficient, more efficient in particular than any potential solar equivalent (like that associated with the production of solar intranetwork fields for instance, if the suspicion that such small-scale features are generated through a distributed solar dynamo is confirmed). An obvious explanation for this enhanced efficiency is the larger rotation rates. It indicates in particular that distributed dynamos like those we observed (but also those of fully convective stars) are therefore not purely turbulent dynamos (as proposed in particular by Durney et al. 1993) as such dynamos are not expected to depend on rotation nor to contribute significantly to the large-scale field structure.

An obvious concern for distributed dynamos is of course to understand how such strong large-scale fields can be retained within the convective zone for time-scales longer than the duration of a typical activity cycle. This non-trivial point is still a matter of intense debate. One can imagine that part of the azimuthal field generated close to the surface is pumped down by convective downdrafts (e.g. Nordlund et al. 1992) or simply transported by meridional circulation (Choudhuri et al. 1995) and stored below the convection zone. Alternatively (or simultaneously), one can imagine that the large-scale field (or at least a significant fraction) is continuously regenerated over time-scales of about one month, as is probably the case for the Sun for instance (e.g. Stenflo 1994).

If the above interpretation is correct, sequences of magnetic images such as that presented here (but spanning a complete magnetic cycle) should inform us on how the large-scale poloidal and toroidal field components evolve with time. From the present data set, we can already see that the field structure of HR 1099 has progressively evolved from an almost purely azimuthal field topology at epoch 1990.9 to a mixed field distribution at following epochs, indicating that the underlying activity cycle is probably in the phase of regenerating the poloidal component of the large-scale dynamo field. Similarly, the appearance of a counterclockwise azimuthal field region at high latitudes on LQ Hya at epoch 1996.99 (if confirmed in future observations) may announce a global polarity switch, just as it does for radial fields on the Sun (Stenflo 1991) for instance. Assuming these large-scale toroidal field structures we detect do indeed reverse their polarity, the fact that no complete polarity switch has yet been observed indicate that our data do not span more than half of a magnetic cycle, implying cycle periods of at least 10 and 12 yr for LQ Hya and HR 1099 respectively.

Our observations also suggest that the axisymmetric spherical harmonic degree of the large-scale magnetic field varies with rotation rate and convective depth. Going from LQ Hya to AB Dor, the large-scale toroidal field component evolves from a primarily dipolar configuration to one with a dominant axisymmetric spherical harmonic component of (presumably odd) degree $\ell \geq 5$ (Donati et al. 1998), whereas the essential difference in stellar fundamental parameters is the rotation rate (3.2 times larger in AB Dor). Note that this behaviour is in qualitative agreement with the conclusions of Schatzmann (1991). It also strengthens the idea outlined above that the distributed dynamos we observed do depend on rotation and are therefore not purely turbulent dynamos. Going from LQ Hya to HR 1099, a similar evolution is observed for both poloidal and toroidal field structures, which suggests that the increase in convective depth between a K0V and a K1IV structure more than compensates the decrease in rotation rate (by a factor of about 1.8). This is very reminiscent of the results obtained by Kitchatinov & Rüdiger (1995) or Schüssler (1996) on the respective effects of rotation and effective temperature on radial differential rotation or magnetic flux rising trajectories within the convective zone of late-type stars.

Finally, it is interesting to note (although perhaps totally meaningless) that the parallel drawn above between the stellar magnetic features we detected and solar intranetwork fields can be extended somewhat further. In addition to the fact that both types of features

are produced within the convective zone proper, we observe that they do not correlate (or only very weakly) with surface brightness inhomogeneities (Lites et al. 1996) and are *not* confined to a restricted range of latitudes. Although the most recent results on intranetwork fields tend to indicate that they do not significantly vary with local activity at the surface of the Sun *at a given epoch*, there is actually no systematic study of their actual dependence with the solar activity cycle yet (Lin 1995). If it turns out that these small-scale solar features do vary with the activity cycle, it would then strongly suggest that the stellar magnetic fields we observed are *scaled-up versions of solar intranetwork fields*. It may in turn strengthen Stenflo's (1994) proposition that these intranetwork fields (and therefore the underlying distributed dynamo) are not due to a pure turbulent dynamo, and do significantly contribute to the large-scale field of the Sun just as they do on other rapidly rotating late-type stars.

5.3 Orbital period variations in HR 1099

As described in Section 3.1.1, our spectropolarimetric data on the RS CVn system HR 1099 demonstrate that, while the system radial velocity and velocity amplitudes remain constant (within better than 0.5 km s^{-1}), the orbital phase of the first (and second) conjunction is slowly varying with time (see Fig. 1). It is already clear from this plot that this variation is not linear with time and is therefore not simply the result of an error in the assumed orbital period. (This error would need to be of the order of 2×10^{-4} d, and would be incompatible with the error bar published by Fekel and also with Mt Wilson observations obtained more than 70 yr ago.) A function with non-zero second derivatives (like a sine curve with a period of 18 ± 2 yr, see Fig. 1) can reproduce the observed fluctuation much better (i.e. within the error bars).

The first natural idea that comes to mind is that HR 1099 (as a system) orbits around a third object in a period of about 18 yr, and that the apparent fluctuations in conjunction time are actually caused by the variation in distance (and therefore in light travel time) between the Earth and HR 1099 as the binary orbits the third body. In this context, the peak-to-peak amplitude of the conjunction time variations (5.4±0.4 per cent) translates into peak-to-peak distance variations of 26.6 ± 2.0 au. Assuming a circular orbit, the observed period of 18 ± 2 yr implies that the systemic radial velocity of HR 1099 should vary with a peak to peak amplitude of about 44 km s^{-1}, totally incompatible with our observations (indicating that the systemic velocity is constant with time up to an accuracy of about 0.5 km s^{-1}) as well as with earlier ones (Fekel 1983). Of course, some of the above estimates (and in particular the orbit period) may be inaccurate, especially if the orbit of HR 1099 around the third body is strongly eccentric and not circular (as implicitly assumed through the sinusoidal fit). However, the discrepancy between predicted and observed systemic radial velocity curves is so large that it makes this scenario extremely unlikely. Note that it also suffers from other severe problems. In particular, the orbit period also implies a minimum mass of 7.3 $M_\odot$ for the third body, which would then need to be some kind of low-mass black hole to explain the fact that it is simply not seen within about 0.5 arcsec of HR 1099 itself.

We therefore have to look for an explanation within the close binary system itself. As $\partial\phi_0/\partial t$ is directly proportional (for a circular orbit) to the deviation of the system orbital period from its nominal value, our findings that ϕ_0 is a function with non-zero second derivatives suggests that the orbital period is truly time variable (by an amount of about 0.015 per cent peak-to-peak), on a time-scale of just a few years. They already indicate that the orbital period was nominal (i.e. equal to 2.83774 d) sometime in 1990 (i.e. when the conjunction phase peaks at about 0.8 per cent) and reached a minimum value of about 2.83753 d at the end of 1994 (when the curvature of the conjunction phase variations switched from negative to positive).

It is of course too early to conclude about the exact shape of long-term time dependence of these fluctuations in orbital period. Assuming the observed variation in the orbital phase of both conjunctions is indeed periodic (as suggested by the sinusoidal fit of Fig. 1), the orbital period would then also be modulated with the same period. Note that such a periodic behaviour of the system orbital period could reconcile in particular the variations we just detected with the fact that this period is constant *on average* on a time-scale of at least 70 yr (Fekel 1983). If we further assume that the observed modulation in conjunction phase obeys a sine law (with a period of 18±2 yr and a peak-to-peak amplitude of 5.4±0.4 per cent), the orbital period should also vary sinusoidally (in phase quadrature and with an amplitude of about $4.2 \pm 0.1 \times 10^{-4}$ d or 36 ± 1 s peak-to-peak), with 1994.8±0.2 as the epoch of orbital period minimum (see Fig. 14). Our observations therefore suggest that the system undergoes periodic phases of *contraction* (like that up to epoch 1994.8, associated with a decrease in orbital period), followed by phases of expansion (from epoch 1994.8 on, associated with an increase in orbital period).

Similar orbital period fluctuations have already been detected in various RS CVn systems, as well as in several other types of objects such as Algol systems, cataclysmic variables and contact binaries (Hall 1990). These orbital period fluctuations usually have a relative semi-amplitude of a few times 10^{-5} and occur on time-scales from less than one decade up to more than one century. Our observations demonstrate for the first time that HR 1099 now belongs to the class of binary systems that show such orbital period fluctuations. To our knowledge, this is the first time that such fluctuations have been detected in a RS CVn system through spectroscopic (rather than photometric) observations. The period of these fluctuations ($P_{\rm mod} = 18 \pm 2$ yr) is one of the shortest known to date, while their peak-to-peak relative amplitude (0.015 per cent) is also one the largest ever detected.

For most of these objects, the third body scenario can be excluded for very similar reasons to those mentioned above. Similarly, all

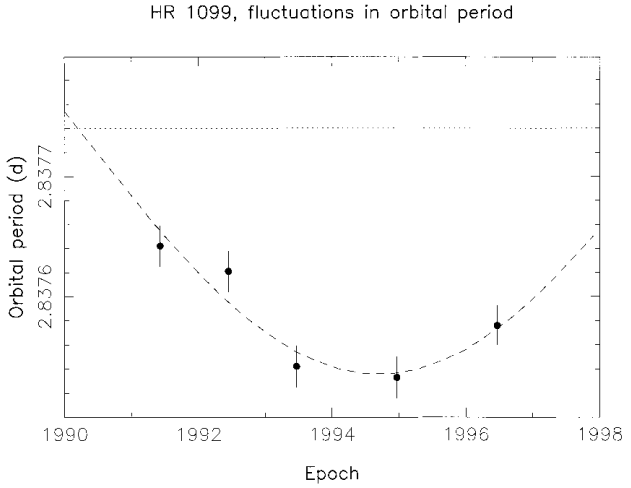

Figure 14. Fluctuations in the orbital period of the RS CVn system HR 1099 (dots). The dashed curve depict the oscillations about the nominal period of 2.83774 d (dotted line) that correspond to the sinusoidal fit of Fig. 1.

mechanisms invoking mass transfer and/or mass loss proposed to date (e.g. Biermann & Hall 1973; DeCampli & Baliunas 1979) have been dismissed on either theoretical or observational arguments (or both). Tidal or magnetic coupling between system components do not seem to be a likely explanation either. Stellar structure models from Charbonnel et al. (1996) indicate that a K1 subgiant with fundamental parameters such as those derived in Section 3.1.2 should be close to entirely convective, with a convective envelope occupying about 75 and 85 per cent of the total stellar mass and radius respectively, a squared gyration radius of 0.13 and an apsidal motion constant k_2 of about 0.06. As departures from synchronization remain always very small in the case of HR 1099, the tidal period is much longer than both tidal friction time and convective turnover time, implying that a rather accurate synchronisation timescale can be derived for HR 1099 from equations (7), (15) and (20) of Zahn (1989). The value we obtain (190 yr) is still about one to two orders of magnitude too large to explain the orbital period fluctuations we observe for HR 1099. Similarly, the large-scale poloidal field of the primary system component, although two orders of magnitude stronger than solar, is still far too weak to produce an efficient magnetic torque. The magnetic energy associated with the field lines of the primary star at the distance of the secondary component (where the field strength is of the order of 10 G, see Section 5.1) is indeed about 10 orders of magnitude smaller than the amount of energy apparently associated with the observed orbital period variations (1.5×10^{43} erg every half-cycle).

The only solution we are left with is that these fluctuations are a result of changes in the *quadrupole moment* of the primary star, and therefore in its gravitational field itself (Matese & Whitmire 1983; Applegate & Patterson 1987; Applegate 1992). In this scenario, there is no coupling of any sort between system components, implying that the orbital angular momentum is conserved, just as the spin angular momentum of both components are. The attractive point is that quadrupole moment changes of the primary star have instant consequences on the motion of the companion (through the modification of the gravitational field itself), with no additional delays for the effect to settle like in the case of tidal interaction for instance. According to Applegate & Patterson (1987) and Applegate (1992), these quadrupole moment changes are a direct consequence of magnetic activity. There is indeed empirical evidence for that, as demonstrated by Hall (1990) who discovered that all systems subject to such orbital period fluctuations do indeed involve one active star with a deep convective zone. Another piece of evidence in this direction in the particular case of HR 1099 is that the period of 18 ± 2 yr we obtain for the orbital period fluctuations is in good agreement with an activity cycle period estimate of 16 ± 1 yr derived by Henry et al. (1995) from long-term photometry, as well as with the lower limit derived in Section 5.2.

The problem however is to explain how magnetic activity can generate such quadrupole moment changes. The initial suggestion of Applegate & Patterson (1987) is that a magnetic field at the base of the convective zone induces an additional anisotropic magnetic pressure, thus deforming the equipotential surfaces and the shape of the star. However, Marsh & Pringle (1990) argued that the energy required to drive these changes is larger than what the star can provide given the short time-scale on which they occur, ruling out this simple idea. A few years later, Applegate (1992) proposed another scenario, in which magnetic activity affects the distribution of angular momentum within the active star, and thus its quadrupole moment. Although the original picture by Applegate (in which the magnetic field provides a torque that makes the rotation more or less rigid) does not seem particularly appropriate in the particular case of RS CVn systems (Applegate 1992), a new and apparently more successful scheme has been recently proposed by Lanza, Rodonò & Rosner (1998). The idea is to invoke periodic exchange between magnetic and kinetic energy within the convective zone (as part of the magnetic cycle) as a possible source for modifying the distribution of angular momentum within the star (at constant total spin angular momentum).

Define the quadrupole moment of the star as in Applegate (1992), i.e. by

$$Q = -\frac{2{R_\star}^3}{3G}\Phi_2(R_\star),$$

where Φ_2 denotes the radial part of the second term in the spherical harmonics expansion of the gravitational potential of the active star ($R_\star$ being the radius of the active star and G the universal gravitational constant). The amount of change $\mathrm{d}Q$ the quadrupole moment needs to undergo to account for the observed orbital period fluctuations is given by equation (7) of Applegate (1992), yielding a value of 1.7×10^{52} g cm^2 peak-to-peak in the particular case of HR 1099. One then needs to work out how much angular rotation rates need to be affected to produce such quadrupole moment changes. In practice, Q depends in a very complex way of how mass, magnetic fields and angular rotation velocity are distributed within the star (through the Poisson equation and that describing hydrostatic support in rotating magnetized stars, e.g. Lanza et al. 1998). However, it is possible to derive a rough estimate for the required relative change in angular rotation rate $\mathrm{d}\Omega/\Omega$, through the very simplifying assumption of a rigidly rotating star with constant total (i.e. kinetic and magnetic) energy (see equation 16 of Lanza et al. 1998).

The first result is that the changes in angular rotation rates are very likely not restricted to an interface layer at the base of the convective zone. Using equation (25) of Applegate (1992), we estimate that the maximum quadrupole moment change that a thin layer of mean radius $0.15\,R_\star$, thickness $0.015\,R_\star$ (i.e. about 20 per cent of the pressure scaleheight at the base of the convective zone, e.g. Schüssler 1996) and mass $0.01\,M_\star$ can generate in the gravitational potential of a $0.25\,M_\star$ radiative core is about 10^{49} g cm^2 for an angular rotation rate equal to that at the surface, i.e. more than three orders of magnitude smaller than what we observe. This result is in perfect agreement with those of Section 5.2, concluding that dynamo processes in the K1 subgiant of HR 1099 (and therefore the angular rotation velocity changes that are presumably associated) are distributed throughout the whole convective zone, rather than being confined in an overshoot interface layer with the radiative interior. If we now assume that the whole convective zone is responsible for the observed quadrupole moment changes, we obtain from equation (16) of Lanza et al. (1998) that $\mathrm{d}\Omega/\Omega$ is equal to ± 1.4 per cent in the particular case of HR 1099.

Photometric observations (measuring temporal variations in photometric period, possibly caused by starspot migration in the presence of differential rotation, and/or to surface changes in angular rotation rate) actually suggest an upper limit of only 0.6 per cent peak-to-peak for $\mathrm{d}\Omega/\Omega$ (Henry et al. 1995), between four and five times smaller than the above estimate. We nevertheless conclude that the agreement with observations is reasonable. One should indeed keep in mind that the above estimate of $\mathrm{d}\Omega/\Omega$ is still fairly rough (as it relies on the assumption of solid rotation for instance, which is strictly speaking incompatible with conservation of total spin angular momentum); if more accurate ones (computed from detailed stellar structure models) would certainly be welcome, they would still be rather uncertain (by at least a factor of two)

unless complete information is available on both magnetic fields and angular rotation rate within the star (e.g. Paternò, Sofia & Di Mauro 1996 in the case of the Sun). In any case, the agreement we obtain with this scenario is far better than with any others, and we thus conclude that it is the less unlikely option to explain our observations.

If we assume that the actual relative changes in angular rotation velocity are about ± 0.3 per cent in the particular case of HR 1099 (i.e. the upper limit that photometric observations allow), the associated variation in kinetic energy (of the order of $I\mathrm{d}\Omega^2$ if we assume spin angular momentum conservation, where I is the moment of inertia of the primary star) is 10^{41} erg. The average azimuthal field strength associated with this variation in kinetic energy is equal to 6 kG. As radial gradients in field intensity certainly exist throughout the convective zone, the expected field at photospheric level is probably of the order of one kG, in good agreement with what we actually measure on this star (see Section 3). The maximum power associated with these kinetic to magnetic energy transfers is about 5 per cent of the total stellar luminosity (peak-to-peak), which verifies a posteriori that Marsh & Pringle's (1990) argument does not apply in our particular case.

6 CONCLUSIONS AND PROSPECTS

We presented in this paper a 6-yr time-series of magnetic (and brightness) surface images of the K1 subgiant of the RS CVn system HR 1099 and of the young K0 dwarf LQ Hya, reconstructed (with the help of a dedicated maximum entropy image reconstruction software) from Zeeman–Doppler imaging observations collected at the Anglo-Australian Telescope (Donati et al. 1997).

The first important result we obtain is that all stellar magnetic images we reconstruct host at least one high-contrast feature in which the field is predominantly azimuthal, thus confirming that such surface structures (already detected by Donati et al. 1992b; Donati & Cameron 1997 and Donati et al. 1999) are indeed real. We take this as strong evidence that the associated dynamo processes operate throughout the whole stellar convective envelope, and not only in an interface layer between the convective and radiative zones as in the Sun. Moreover, the magnetic regions that we detect show very weak spatial correlation with surface brightness inhomogeneities and do not seem to be confined to a restricted latitude range, suggesting that they could be scaled up analogues of solar intranetwork fields (rather than active regions).

The latitudinal polarity pattern of azimuthal and radial fields that we observe at the surface of both stars suggest that these magnetic regions respectively witness the toroidal and poloidal components of the large-scale dynamo field. The spatial structure of these two magnetic field components gets increasingly more complex (with higher axisymmetric spherical harmonic degrees) for larger rotation rates and deeper convective zones. The strength of these toroidal and poloidal components is typically a few hundred G, more than two orders of magnitude stronger than in the Sun. Long-term evolution of the large-scale field structure (and of the toroidal and poloidal components in particular) is clearly detected.

We also report the detection of small fluctuations in the orbital period of HR 1099, with a peak-to-peak amplitude of about 36 ± 1 s (i.e. 0.015 per cent) and a period of about 18 ± 2 yr (assuming sinusoidal variations around the nominal value). The most plausible way of explaining such fluctuations is that the quadrupole moment of the K1 subgiant is varying with time, and that this modulation is driven by the magnetic activity cycle of the primary star itself. Our observations thus give further support to the model of Applegate (1992) in its most recent adaptation (Lanza et al. 1998), which proposes that periodic exchange between kinetic and magnetic energy within the convective zone and throughout the activity cycle is responsible for changes in the internal angular rotation rate and thus in the quadrupole moment of the active star. It provides in particular an independent confirmation that dynamo operates within the whole convective zone, and suggests that the average azimuthal field in this convective envelope is of the order of 6 kG.

This study is of course the beginning of a longer term one, aimed at monitoring cyclic evolution of the large-scale dynamo field structures of a few selected active stars throughout the HR diagram. The obvious goal is to follow the time distortion of both poloidal and toroidal components of the large-scale magnetic field over at least one complete activity cycle (and possibly more), focusing for instance on potential sign switches of these two components, equatorward/poleward migration patterns at the stellar surface, or variable angular tilt between the magnetic and rotation axes. Another interesting possibility would be to perform harmonic analyses on time series of the axially symmetric component of stellar magnetic topologies, just as Stenflo (1992) did in the particular case of the Sun. More generally, we plan to collect *solar-like* observations of dynamo magnetic structures for various objects throughout the Hertzsprung–Russell diagram (sampling in particular a wide range of ages, effective temperatures and rotation rates), with the ultimate goal of obtaining a unified theory for solar and stellar dynamo processes.

Monitoring surface differential rotation patterns (Donati & Cameron 1997) and in particular possible modulation of this differential rotation with the activity cycle should also help, not only in trying to test in further details the model Lanza et al. (1998) proposed for explaining orbital period fluctuations of binary systems, but also in identifying the essential physical ingredients at the origin of differential rotation within stellar convective zones. A modulation with stellar activity would confirm at least that magnetic field has a definite impact on the internal angular rotation rate of active stars, and that differential rotation is therefore not a purely hydrodynamical process as originally assumed by Kitchatinov & Rüdiger (1995) or Rüdiger et al. (1998). This is precisely the kind of information one needs to collect in order to construct, ultimately, a self-consistent dynamo theory that reproduces *all* observational constraints (e.g. topology of toroidal and poloidal components of large-scale field structure, differential rotation, quadrupole moment changes) at the same time.

ACKNOWLEDGMENTS

We thank Meir Semel, Olivier Durand, Brad Carter, Matthew Mengel, Andrew Cameron, Gaitee Hussain and the AAT staff for their help in collecting the yet unpublished 1996 December observations of HR 1099 and LQ Hya. We also gratefully acknowledge John Landstreet, Katia Ferriere, Antonino Lanza, Michel Rieutord and Claude Catala for useful discussions on some aspects presented in this paper, as well as André Mangeney for a key comment on early observations from which this study is inspired. We also thank Corinne Charbonnel for providing us with internal stellar structure models corresponding to the two stars we focused on, and the referee, Artie Hatzes, for making comments and suggesting several modifications that improved and clarified the paper. This work is based on data collected with the UCL Echelle spectrograph at the Anglo-Australian Telescope.

REFERENCES

Applegate J. H., 1992, ApJ, 385, 621
Applegate J. H., Patterson J., 1987, ApJ, 322, L99
Biermann P., Hall D. S., 1973, A&A, 27, 249
Borra E. F., Landstreet J. D., 1980, ApJS, 42, 421
Brandenburg A., Charbonneau P., Kitchatinov L. L., Rüdiger G., 1994, in Caillault J.-P., ed., PASP Conf. Ser. 64, 8th Cambridge Workshop on Cool Stars, Stellar Systems and the Sun. Astron. Soc. Pac., San Francisco, p. 354
Bressan A., Fagotto F., Bertelli G., Chiosi C., 1993, A&AS, 100, 647
Brown S. F., Donati J.-F., Rees D. E., Semel M., 1991, A&A, 250, 463
Cameron A. C., 1992, in Byrne P. B., Mullan D. J., eds, Surface Inhomogeneities on Late-Type Stars. Springer, Berlin, p. 33
Cameron A. C., Unruh Y. C., 1994, MNRAS, 269, 814
Charbonnel C., Meynet G., Maeder A., Schaerer D., 1996, A&AS, 115, 339
Choudhuri A. R., Schüssler M., Dikpati M., 1995, A&A, 303, L29
DeCampli W. M., Baliunas S. L., 1979, ApJ, 230, 815
DeLuca E. E., Fan Y., Saar S. H., 1997, ApJ, 481, 369
Donati J.-F., 1996a, in Strassmeier K. G., Linsky J. L., eds, Proc. IAU Symp. 176, Stellar Surface Structure. Kluwer, Dordrecht, p. 53
Donati J.-F., 1996b, in Donati J.-F., ed., 3rd AFCOP workshop, Solar & Stellar Dynamos, Constraints from Observations. Corep, Toulouse, p. 83
Donati J.-F., Brown S. F., 1997, A&A, 326, 1135
Donati J.-F., Brown S. F., Semel M., Rees D. E., Dempsey R. C., Matthews J. M., Henry G. W., Hall D. S., 1992, A&A, 265, 682
Donati J.-F., Cameron A. C., 1997, MNRAS, 291, 1
Donati J.-F., Cameron A. C., Hussain G. A. J., Semel M., 1999, MNRAS, 302, 437 (Paper I, this issue)
Donati J.-F., Semel M., Carter B. D., Rees D. E., Cameron A. C., 1997, MNRAS, 291, 658
Donati J.-F., Semel M., Rees D. E., 1992a, A&A, 265, 669
Durney B. R., De Young D. S., Roxburgh I. W., 1993, Solar Phys., 145, 207
Fekel F. C., 1983, ApJ, 268, 274
Hall D. S., 1990, in Ibanoglu C., ed., Active Close Binaries. Kluwer, Dordrecht, p. 95
Henry G. W., Eaton J. A., Hamer J., Hall D. S., 1995, ApJS, 97, 513
Jankov S., Donati J.-F., 1995, in Huang L., Zhai D. S., Catala C., Foing B. H., eds, Proc. 4th MuSiCoS workshop, p. 143
Kitchatinov L. L., Rüdiger G., 1995, A&A, 299, 446
Kurucz R. L., 1993, CDROM # 13 (ATLAS9 atmospheric models) and # 18 (ATLAS9 and SYNTHE routines, spectral line database)
Lanza A. F., Rodonò M., Rosner R., 1998, MNRAS, 296, 893
Lin H., 1995, ApJ, 446, 421
Lites B. W., Leka K. D., Skumanich A., Martínez Pillet V., Shimizu T., 1996, ApJ 460, 1019
MacGregor K. B., Charbonneau P., 1997, ApJ, 486, 484
Marsh T. R., Pringle J. E., 1990, ApJ, 365, 677
Matese J. J., Whitmire D. P., 1983, A&A, 117, L7
Nordlund Å., Brandenburg A., Jennings R. L., Rieutord M., Ruokolainen J., Stein R. F., Tuominen I., 1992, ApJ, 392, 647
Parker E. N., 1993, ApJ, 408, 707
Paternò L., Sofia S., Di Mauro M. P., 1996, A&A, 314, 940
Perryman M. A. C. et al., 1997, A&A, 323, L49
Robinson R. D., 1980, ApJ, 239, 961
Rüdiger G., von Rekowski B., Donahue R. A., Baliunas S. L., 1998, ApJ, 494, 691
Schatzman E., 1991, in Cox A. N., Livingston W. C., Matthews M. S., eds, Solar Interior and Atmosphere. Univ. Arizona Press, p. 192
Schüssler M., 1996, in Strassmeier K. G., Linsky J. L., eds, Proc. IAU Symp. 176, Stellar Surface Structure. Kluwer, Dordrecht, p. 267
Semel M., 1989, A&A, 225, 456
Semel M., Li J., 1995, Solar Phys., 164, 417
Skilling J., Bryan R. K., 1984, MNRAS, 211, 111
Stenflo J. O., 1992, in Tuominen I., Moss D., Rüdiger G., eds, Proc. IAU Coll. 130, The Sun and Cool Stars: Activity, Magnetism, Dynamos. Springer, Berlin, p. 193
Stenflo J. O., 1994, in Ap&SS Lib. 189, Solar Magnetic Fields, polarised radiation diagnostics. Kluwer, Dordrecht, p. 20
Strassmeier K. G., Rice J. B., Wehlau W. H., Hill G. M., Matthews J. M., 1993, A&A, 268, 671
Strassmeier K. G., Bartus J., Cutispoto G., Rodonò M., 1997, A&AS, 125, 11
Vogt S. S., Hatzes A. P., Misch A. A., Kürster M., 1998, ApJS, in press
Zahn J.-P., 1989, A&A, 220, 112

This paper has been typeset from a TEX/LATEX file prepared by the author.